Agenzia nazionale per le nuove tecnologie,
l'energia e lo sviluppo economico sostenibile

MINISTERO DELLO SVILUPPO ECONOMICO

Ricerca di Sistema elettrico

Risultati relativi alle campagne sperimentali di breve e medio termine sui fenomeni di erosione/corrosione da litio liquido fluente nell'impianto Lifus 6

P.Favuzza, M.Cuzzani, G. Fasano

Report RdS/PAR2015/179

RISULTATI RELATIVI ALLE CAMPAGNE SPERIMENTALI DI BREVE E MEDIO TERMINE SUI FENOMENI DI EROSIONE/CORROSIONE DA LITIO LIQUIDO FLUENTE NELL'IMPIANTO LIFUS 6

P. Favuzza	FSN-ING-QMN	Enea Firenze
M. Cuzzani	FSN-ING-TESP	Enea Brasimone
G. Fasano	FSN-ING-TESP	Enea Brasimone

Settembre 2016

Report Ricerca di Sistema Elettrico

Accordo di Programma Ministero dello Sviluppo Economico - ENEA
Piano Annuale di Realizzazione 2015
Area: GENERAZIONE DI ENERGIA ELETTRICA CON BASSE EMISSIONI DI CARBONIO
Progetto: B.3.2 – Attività di Fisica della Fusione Complementari a ITER
Obiettivo: *B1* - F*orniture ed implementazioni comuni per progettazione, costruzione ed operazioni riguardanti gli impianti a litio ELTL e LiFus6 per attività sperimentali su corrosione/erosione, purificazione, termoidraulica e cavitazione per IFMIF*
Responsabile del Progetto: A. Pizzuto, ENEA

Si ringrazia il dott. Stefano Caporali del *Consorzio Interuniversitario Nazionale Per La Scienza E Tecnologia Dei Materiali* per il supporto fornito nell'analisi chimica-metallografica dei provini utilizzati nel corso della campagna sperimentale.

Indice

Sommario

This report deals with the results of the erosion-corrosion tests executed during the last year in ENEA Brasimone centre with the Lifus 6 plant; this activity was performed in the framework of the task LF03 of the IFMIF project. These tests entail to expose specimens made of Eurofer 97 and F82H, which are RAFM (Reduced Activation Ferritic Martensitic) steels, to the action of liquid Lithium flowing at 15 m/s and 330°C, in purity controlled conditions (Nitrogen concentration in Lithium ≤ 30 wppm). The whole experimental activity is composed of three tests differing only in the exposure duration (a short one, a mid one and a long one), up to a maximum time of 4000 hours.

In this report are presented the results of the first two tests, the short term one, covering a duration of 1222 hours, and the mid term one, covering a duration of 2000 hours. The outcome of the short test is largely discussed, on the basis of both the mass variation of the specimens and their chemical, optical and metallographic investigations; for what concerns the mid test, only a preliminary assessment is instead possible, based on the registered mass variations, being still ongoing all the other kinds of analyses.

On the whole, it can be said that the short test results are quite comforting, since the maximum registered corrosion rates was ~ 0.23 µm/y, a value significantly smaller than the corrosion rate limit set for IFMIF (1 µm/y). The optical and SEM analyses of both the exposed surfaces and the cross sections of the specimens confirm the good behaviour of the materials, since no alteration of the morphology or of the grain structure is evident. Only a minimal decrease of Chromium (Cr) concentration at the surface after the test was evidenced, on the average by ~ 1% by weight.

The mass variations of the mid term specimens were again very small and translated likewise in small corrosion rates; only one specimen exhibited the relatively larger value of ~ 0.76 µm/y, probably in view of some Lithium flow turbulence in the specific position where it had been located.

Next analyses and the future long term test are called to verify and confirm these results and the good behaviour of the investigated steels.

1 Introduzione

Lifus 6 plant was designed and constructed during the past years in ENEA Brasimone centre in order to perform erosion-corrosion resistance tests of steels specimens, when exposed to flowing liquid Lithium[1,2]; this activity is performed in the framework of the LF03 task of the IFMIF project. Limits of the corrosion rate were specified by the IFMIF Comprehensive Design Report [3] as follows:

- 1 µm per year in the target
- 50 µm over 30 years in the rest of loop

A part from the components general thinning and the formation of wandering corrosion products in Lithium, local shape modifications due to erosion-corrosion could generate flow instabilities and lead to irregular Lithium film thickness or massive spills, causing in turn the beam trip off and the stop of the IFMIF plant operation.

Lifus 6 experimental activity collects the heritage of a first exploratory run performed during 2007 with the LIFUS 3 plant in ENEA Brasimone Centre, in which both AISI 316 and Eurofer 97 specimens were put in contact for 1000 hours with liquid Lithium, flowing at 350°C and 16 m/s, but without a measured purity level [4]. In order to overcome this limit and to dispose of Lithium with controlled impurities amounts, so to comply with IFMIF operations, the LF03 task has indicated to realize a new, improved Lithium plant (Lifus 6), featuring also a purification system, consisting of:

- a Cold Trap, aimed at reducing Carbon and Oxygen concentration in Lithium below 10 wppm and Hydrogen one to about 60 wppm;
- an Hot Trap, aimed at reducing Nitrogen concentration in Lithium below 30 wppm;
- a Resistivity Meter, aimed at continuously monitoring the total impurity content in flowing Lithium;
- a sampling unit, allowing to take few grams of Lithium from the plant and to perform a specific batch chemical analysis on it, to precisely quantify the concentration of Nitrogen, the most corrosion affecting impurity.

(the realization and the validation of the Lifus 6 purification system [5-8] is the subject of another dedicated IFMIF task, the LF 04-EU PA Procurement Arrangement).

The following test grid has been established for the entire erosion-corrosion experimental campaign assigned to Lifus 6 plant:

Table 1: Grid of corrosion tests. Velocity, Temperature and Nitrogen refer to Lithium properties; Roughness refers instead to specimens surface

Run	Material	Duration [h]	Velocity [m/s]	Temperature [°C]	Nitrogen [wppm]	Roughness Ra [µm]	Investigated specimens
Short term	Eurofer 97 + F82H	1000	15	330	< 30	< 3.0	8 (4+4)
Mid term	Eurofer 97 + F82H	2000 ÷ 3000	15	330	< 30	< 3.0	8 (4+4)
Long term	Eurofer 97 + F82H	4000 ÷ 6000	15	330	< 30	< 3.0	4 (2+2)

On the whole, three different tests are scheduled, involving two different Reduced Activation Ferritic-Martensitic (RAFM) steels, Eurofer 97 and F82H. The experimental conditions of the three tests are identical: they only differ in terms of duration.

This Report deals with the results of both the short and the mid term test, in terms of the evaluated erosion-corrosion resistance of the exposed specimens. While a complete characterization of the specimens after the short term test is presented, based on the variation of their mass, their surface roughness, their morphology (both by optical and electronic microscopy) and their local chemical composition (by EDS), only a preliminary assessment is made about the effect of the mid term exposure, based on the specimens mass variation, being the related chemical and metallographic analyses still ongoing.

2 Descrizione delle attività svolte e risultati

2.1 Lifus 6 Test Section and specimens general properties

The Test Section is that part of the plant where the investigated specimens are put in contact with the flowing liquid Lithium. Its design is shown in Figure 1.

Lithium, which moves at ~ 30 L/min inside the plant, once entered the Test Section from the top is forced to flow downwards through a thin duct, having an annulus section with ½ mm span. The reduction of the pipe section produces the increase of the metal linear velocity in the duct up to about 15 m/s. The duct is realized by fixing, inside a pipe with an internal diameter of 21 mm (external dimension = 1" standard pipe), 8 specimens having the shape of hollow cylinders, with an outer diameter of 20 mm, an inner diameter (hole for the rod) of 10 mm and a height of 8 mm (see Figure 2). The specimens, aligned one over the other, expose therefore only their external cylindrical surface to the flowing Lithium.

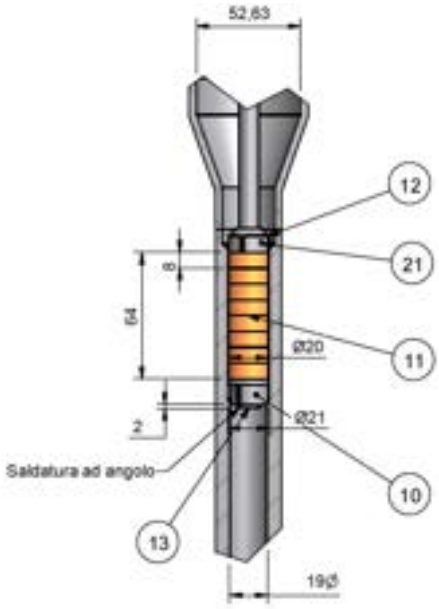

Figure 1: design of Lifus 6 Test Section, highlighting in yellow the specimens disposal. Physical dimensions are expressed in mm

The specimens are mounted on a rod fixed in the upper part to a removable centring plate, and supported on the top and the bottom of the specimens assembly with centring systems. The centring plate is completely uncoupled to the upper flange, to maintain the possibility of easily removing the flange and employing an extraction system for the specimens assembly, which is likely to be stuck at the end of the test, in view of the even small presence of residual Lithium. The triple anchoring of the support rod prevents the occurrence of vibrations in turbulent flow conditions.

Figure 2: appearance of a fresh specimen, from the top

Both the investigated materials are classified as Reduced Activation Ferritic-Martensitic (RAFM) steels, in that they are Iron alloys in which the presence of elements with long decay times due to activation by neutron irradiation (like Ni, Nb, Mo, Al…) must be as much as possible limited. The two materials have a very similar chemical composition, being characterized by about 8-9% by weight of Chromium (Cr) and little amounts of Manganese (Mn), Vanadium (V) and Tungsten (W): the only significant difference lies in the amount of W, which is ~ 2% in F82H, while it is ~ 1% in Eurofer 97. Precise chemical composition of the employed Eurofer 97 and F82H are reported respectively in Table 2 and Table 3, as determined by the producer of the alloys [9]. From a structural point of view, the two materials differ in the grain size, being in the order of 10 µm for the Eurofer 97 and about 50-100 µm for the F82H (clearly these values are not fixed, but may vary according to thermal treatments).

The specimens employed for the Lifus 6 experimental activities have been realized, in ENEA workshop, starting from large plates of the 2 materials. After assuming the right shape, the specimens have been subjected to a proper treatment of the surface exposed to Lithium, to get a roughness suitable for the test (s he a

saarschmiede
Freiformschmiede
66330 Völklingen

GÜTEÜBERWACHUNG

WAZ-Nr.: 6427/1b
Anlage: 1

Kommission: Kunde: EFDA Marke: VIM+VAR 1.4914x3 , EUROFER 97-2

Chemische Zusammensetzung (Gew.-%) (Stückanalyse)

Schmelze-Nr.	C	Si	Mn	P	S	Ni	Cr	Mo	V	Ta	W	Ti	Cu	Nb	Al	N_2	B
Soll	0,090-0,120	< 0,050	0,20-0,60	< 0,005	< 0,005	< 0,01	8,50-9,50	< 0,005	0,15 0,25	0,10-0,14	1,00-1,20	< 0,02	< 0,01	< 0,005	< 0,01	0,015-0,045	< 0,002
993391	0,110	0,031	0,55	0,0010	0,001	0,013	8,95	0,005	0,202	0,120	1,06	0,001	0,005	0,005	0,009	0,022	0,0009

Co	As+Sn+Sb+Zr	O_2
< 0,01	< 0,05	< 0,01
0,004	0,009	0,0007

Table 2. Chemical Composition(wt.%)

Heat No.	Roll No.		C	Si	Mn	P	S	Cu	Ni	Cr	Mo	V	Nb	B	T.N	Sol. Al	Co	Ti	Ta	W
9753		Ladle	0.09	0.08	0.1	0.003	0.001	0.01	0.02	7.89	0.003	0.19	0.0002	0.0002	0.006	0.001	0.003	0.004	0.02	1.99
9753	KG819-2 15t ingot top	check	0.09	0.07	0.1	0.003	0.001	0.01	0.02	7.87	0.003	0.19	0.0002	0.0002	0.006	0.001	0.003	0.004	0.04	1.98
9753	KG819-1 15t ingot middle	check	0.09	0.07	0.1	0.003	0.001	0.01	0.02	7.87	0.003	0.19	0.0002	0.0002	0.007	0.001	0.003	0.004	0.03	1.98
9753	KG820-2 25t ingot middle	check	0.09	0.07	0.1	0.003	0.001	0.01	0.02	7.84	0.003	0.19	0.0002	0.0002	0.007	0.001	0.003	0.004	0.04	1.98
9753	KG820-1 25t ingot bottom	check	0.09	0.07	0.1	0.003	0.001	0.01	0.02	7.82	0.003	0.19	0.0002	0.0002	0.007	0.001	0.002	0.004	0.04	1.98

2.2 Starting specimens characterization

It is of course necessary to characterize each specimen before starting the test, in order to compare it to itself at the end of the test. The physical parameters of the 8 specimens employed in the short term test, as well as the 8 ones employed in the mid term test, have been precisely determined. They are reported in Table 4.

Table 4: physical parameters of the fresh specimens employed for the short and the mid term tests

Material	Sample ID	Height[1] [mm]	External Diameter[1] [mm]	Mass[2] [g]
Short Term Test				
Eurofer 97	2	8.018	19.996	14.73200
Eurofer 97	3	8.017	20.001	14.74337
Eurofer 97	4	8.019	20.000	14.75050
Eurofer 97	5	8.022	19.998	14.74366
F82H	23	8.033	19.999	14.84251
F82H	24	8.035	19.996	14.83910
F82H	25	8.032	19.999	14.83987
F82H	26	8.036	19.998	14.84498
Mid Term Test				
Eurofer 97	6	8.019	20.001	14.75172
Eurofer 97	7	8.022	19.996	14.74200
Eurofer 97	8	8.017	19.997	14.73279
Eurofer 97	9	8.018	20.001	14.74391
F82H	27	8.033	19.998	14.84363
F82H	28	8.035	20.001	14.85061
F82H	29	8.031	20.000	14.84441
F82H	30	8.032	19.999	14.84158

[1] All the specimens are characterized by a parallelism error = 0.002 mm and a diameter ovalization = 0.001 mm

[2] The Std Dev of the measurement is $\leq$ 0.02 mg, as declared by the supplier of the employed balance.

Additionally, one fresh specimen for each material (not devoted to the test) has been instead subjected to the determination of the surface roughness profile, the optical microscope/stereoscope visual inspection, the scanning electron microscope observation (SEM) and the verification of the chemical composition (EDS analysis), as representative of all the specimens of the same material. The results of these investigations, performed in ENEA Brasimone centre, are illustrated by Figures 3 to 5, for Eurofer 97, and Figures 6 to 8, for F82H. It must be underlined that the EDS analysis doesn't provide an extremely accurate composition, in that each element concentrations is commonly affected by an error of about ± 0.5 wt %, the error varying with the specific element; moreover, low mass element (< Fluorine), cannot be correctly quantified. The EDS analyses anyway confirmed that the specimens materials compositions matched the ones in Table 2 and 3.

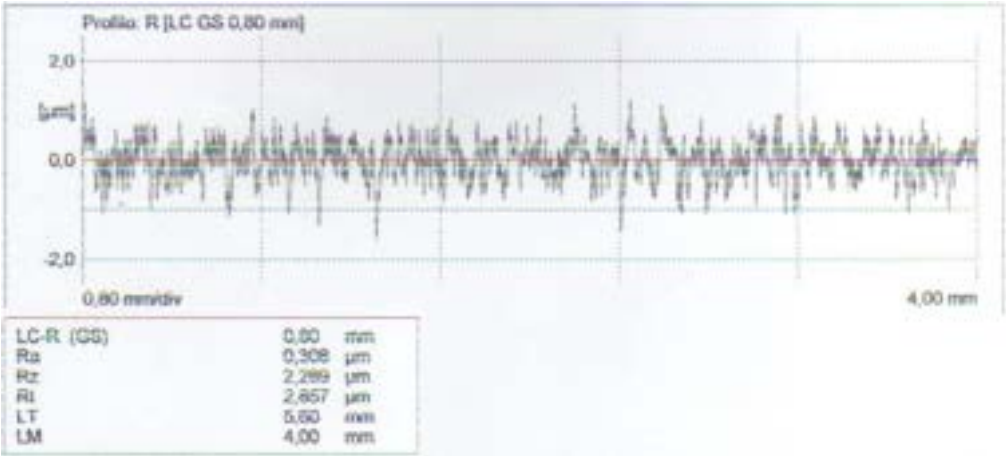

Figure 3: roughness profile of the external surface of a representative Eurofer 97 specimen. It complies with value in Table 1

Figure 4: stereoscope image of a representative Eurofer 97 specimen: curved external surface, viewed from the top. The surface is in good shape.

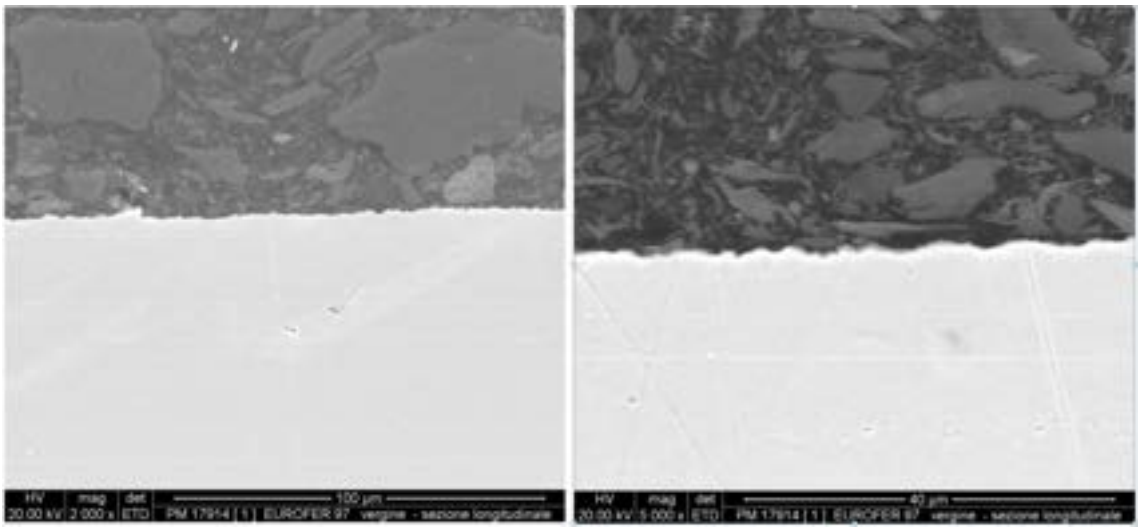

Figure 5: SEM images (secondary electrons) of a representative Eurofer 97 specimen: longitudinal sections. The surface is in good shape (dark region in the top half is due to graphite, where the specimen is mounted in).

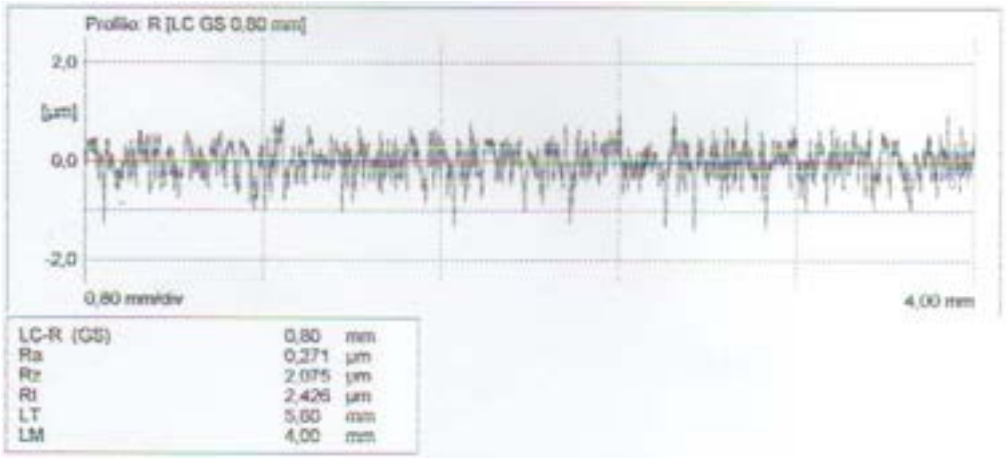

Figure 6: roughness profile of the external surface of a representative F82H specimen. It complies with the value in Table 1

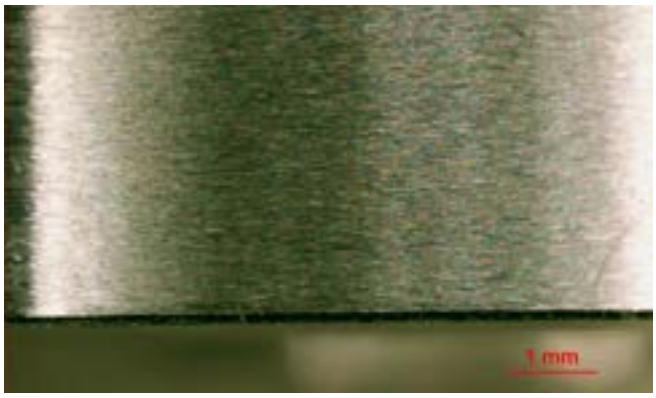

Figure 7: stereoscope image of a representative F82H specimen: curved external surface, viewed from the top. The surface is in good shape.

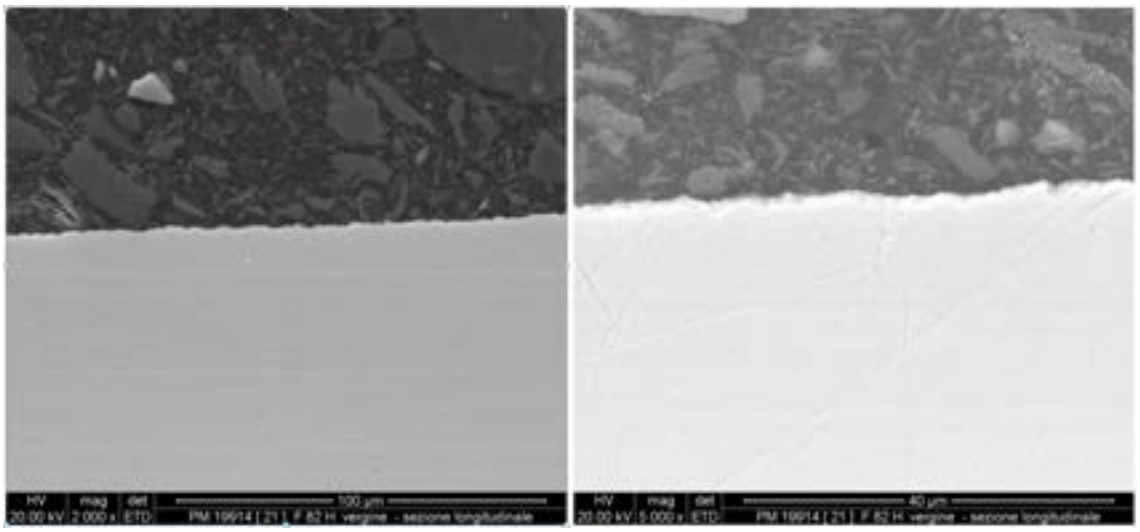

Figure 8: SEM images (secondary electrons) of a representative Eurofer 97 specimen: longitudinal sections. The surface is in good shape (dark region in the top half is due to graphite, where the specimen is mounted in).

2.3 Erosion-corrosion tests execution

For what concerns the short term test, it started around midday of the 17th of November, 2015. According to Table 1, its durations should have been 1000 hours; anyway, since this way it should have been concluded during the last hours of the year, its expiration was slightly postponed to the morning of 7th of January 2016, when Brasimone centre reopened after the X-mas holydays period. Therefore, the actual duration of the Test corresponds to 1222 hours. The mid term test started instead the 9th of March 2016 and terminated the 29th of June, covering an effective duration of 2000 hours.

Both the tests were perfectly accomplished, for what concerns the thermal and dynamic conditions of Lithium in the Test Section: temperature inside the Test Section was registered in the range of 330-331°C during the entire tests period; Lithium flow rate was always in the range of 28-30 L/min, value which assures a metal linear speed of about 15 m/s (only two brief stops of the electricity supply occurred, due to external grid troubles: the longest lasted for 2 hours, after which the proper plant conditions were however quickly restored). Figure 9 shows, as example, the Test Section temperature during the 1222 hours of the short term test; similarly, Figure 10 shows the trend of the Lithium flow rate in the Test Section during the same test.

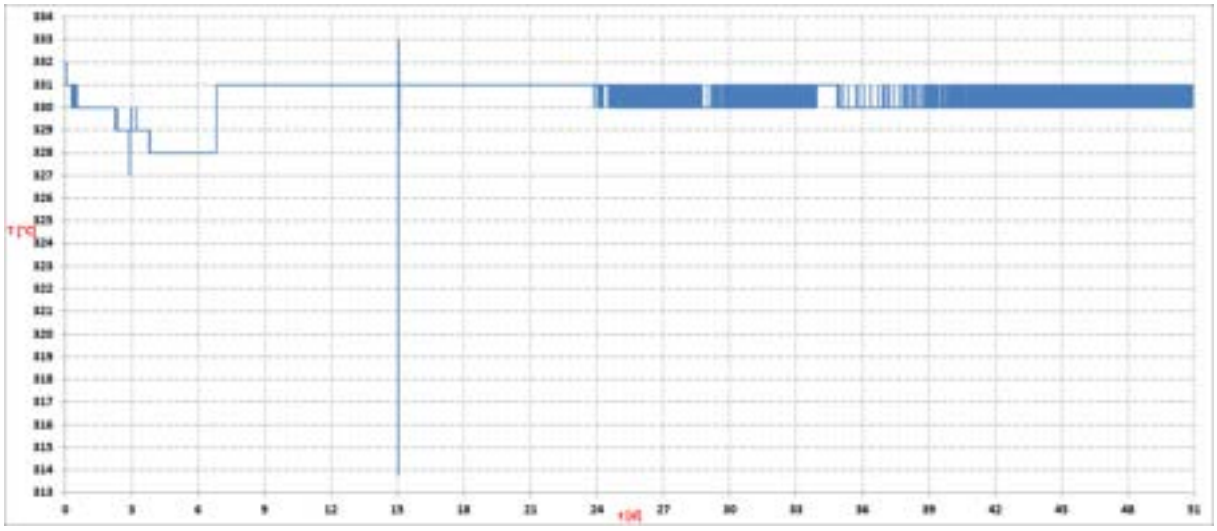

Figure 9: trend of the registered temperature of Lifus 6 Test Section during the short term test (day 15 negative peak corresponds to the momentary decrease due to electricity stop)

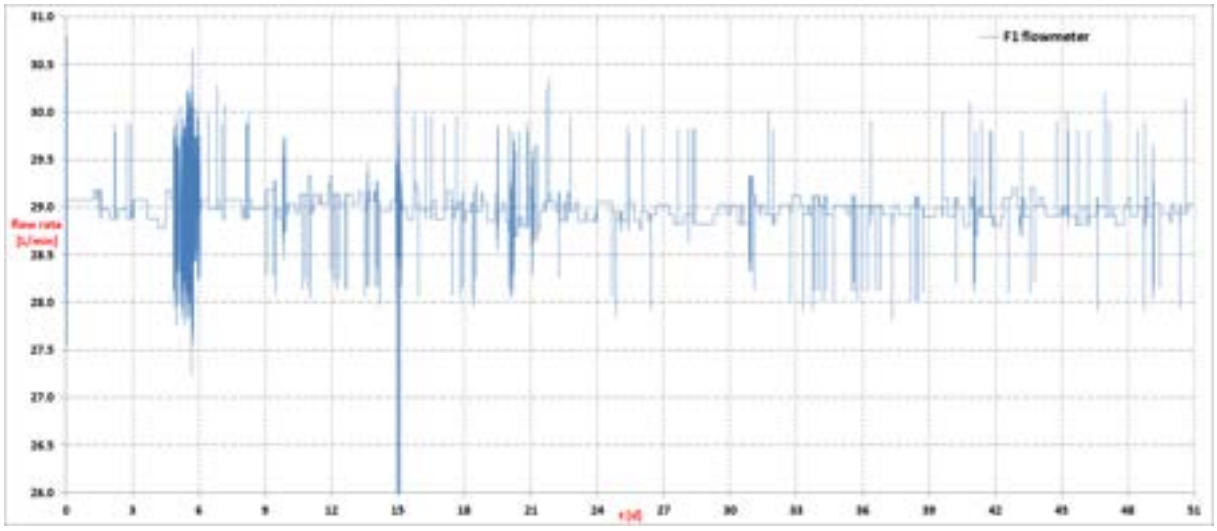

Figure 10: trend of the Li flow rate inside main Lifus 6 loop (and Test Section) during the whole short term test

For what concerns Lithium purity condition, it has been verified as well and shown to comply to the related requirement (Table 1), since during both the short and the mid term Nitrogen concentration in Lithium resulted ≤ 30 wppm. This value was achieved thanks to the employment of the Hot Trap installed in Lifus 6 plant and measured by the offline chemical analyses of samples of Lithium, as well as confirmed by the substantial constancy of Lithium electrical resistivity during the experiments. The details of these measurements and results are reported in [10] and [11] and are the subject of the dedicated report "*Risultati relativi al grado di purezza del litio circolante nell'impianto Lifus 6 ed al funzionamento ed efficienza di dispositivi e procedure per la purificazione*", which accompanies this one.

At the end of each test, the plant was drained and cooled to room temperature. Then the Test Section was opened and the rod holding the specimens was extracted from the top. The operation was performed while flowing Argon from the bottom of the section, to exclude air (lighter than Argon) entering the plant. The specimens were then subjected to a deep characterization to assess the chemical-structural alteration produced by the test.

2.4 Analysis of the specimens after the short term test

2.4.1 Mass variation and generalized corrosion rate

Once removed from the rod, the 8 specimens have been thoroughly washed, by letting them in boiling water for 45 minutes; after drying, the have been weighed.

Table 5 reports the measured mass variations of the 8 specimens, calculated by difference from the values in Table 4. From the knowledge of the mass variation of each specimen, the exact value of the surface exposed to flowing Lithium (given by the product: $\pi * d_e * h$, where d_e and h are respectively the external diameter and the height of the specimen), the densities of the specimens materials (7.9 g/cm^3) and the total time of the test (1222 hours), it is moreover possible to estimate the corrosion rate [µm/y] of the specimens in the specifically applied experimental conditions. This quantity of course provides only a partial indication of the outcome of the test, in that it does not consider the local corrosion phenomenon as well as the possibility of inclusion of external elements in the material lattice, giving instead an average answer, in quantitative terms, of the surface behaviour. It should therefore be better indicate as 'generalized' corrosion rate, as if the specimen material was simply homogeneously dissolved by the flowing metal.

Table 5: mass variation and generalized corrosion rate for the short term specimens

Material	Specimen identification	Mass variation [mg]	Corrosion rate [µm/y]
Eurofer 97	2	- 0.03 ± 0.03*	0.05 ± 0.05
Eurofer 97	3	- 0.13 ± 0.03	0.23 ± 0.05
Eurofer 97	4	+ 0.01 ± 0.03	< 0.05
Eurofer 97	5	- 0.05 ± 0.03	0.09 ± 0.05
F82H	23	- 0.13 ± 0.03	0.23 ± 0.05
F82H	24	- 0.06 ± 0.03	0.11 ± 0.05
F82H	25	- 0.02 ± 0.03	0.04 ± 0.05
F82H	26	+ 0.02 ± 0.03	< 0.05

* ± 0.03 mg is the Standard Deviation of the weighing process

The results shown in table 5 are surely very good, in that mass variations are very small, in most cases close to 0, since similar to the estimated uncertainty in the weighing process. The maximum mass variation translates however into a corrosion rate equal to 0.23 µm/y, which is largely lower than the requirement set for the IFMIF Target material (≤ 1 µm/y). No evident difference is seen between the 2 investigated materials.

2.4.2 Diameter and height variations

The external diameter and the height of each specimens after the test have been precisely determined too. The variations, evaluated respect to the corresponding values of the fresh specimens (Table 4), result for all of them ≤ measure sensitivity (0.001 mm), therefore it can be concluded that no real variation took place. This evidence reflects what expected on the basis of the already reported mass variations.

2.4.3 Optical stereoscope inspection

All the 8 specimens present, after the short term test, a smooth and regular surface, not different from that of the fresh specimens. Figure 11 and 12 show the surface of tested specimens n°2 (Eurofer 97) and n° 23 (F82H), as representative of all the investigated specimens.

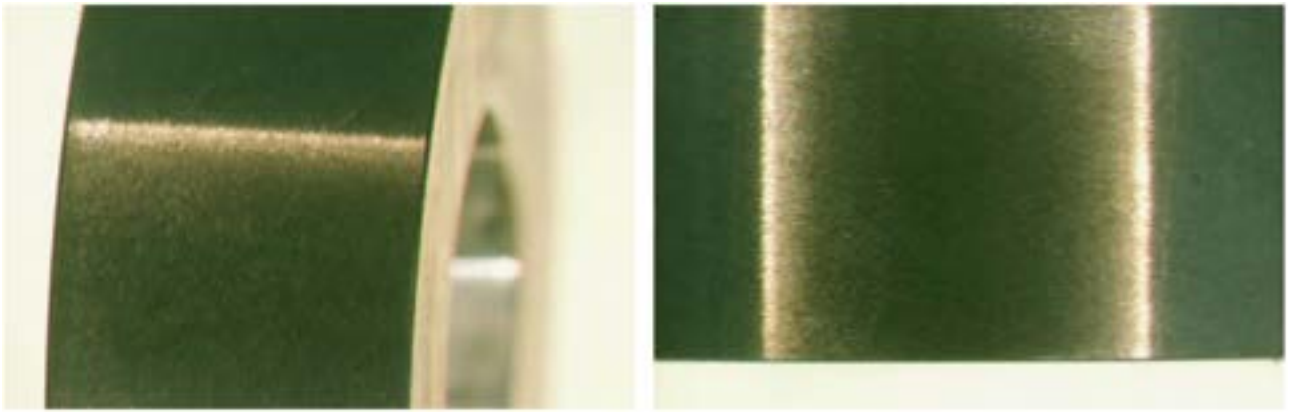

Figure 11: visual inspection of the surface of tested specimen n°2 (Eurofer 97). Left: overall view; right: external (cylindrical) surface, from the top

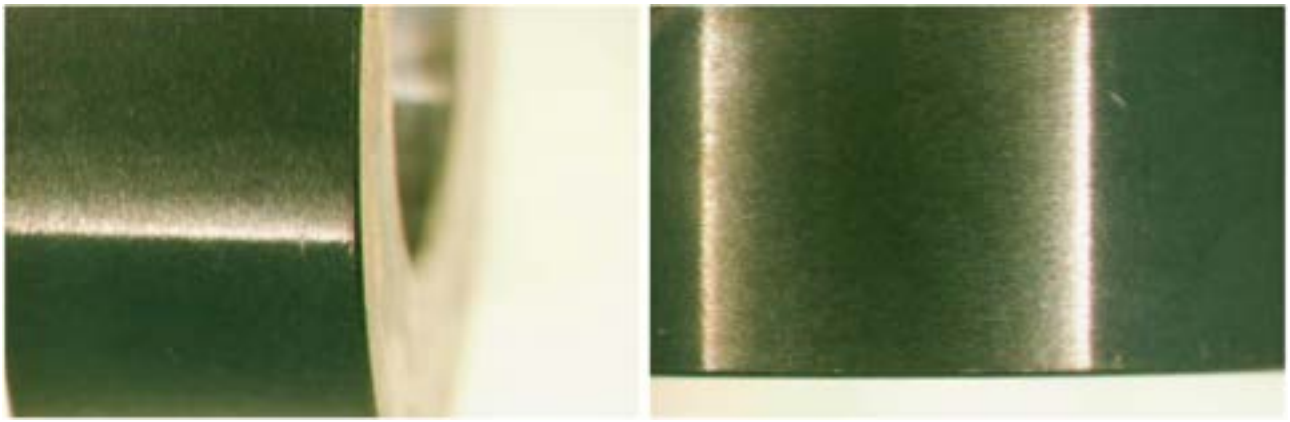

Figure 12: visual inspection of the surface of tested specimen n°23 (F82H). Left: overall view; right: external (cylindrical) surface, from the top

2.4.4 Roughness profile of the specimens

The roughness profiles of all the 8 investigated specimens have been measured at the end of the erosion-corrosion test. The Ra parameter results 0.275, 0.306, 0.313, 0.289 µm respectively for specimen n° 2,3,4,5 (Eurofer 97) and 0.293, 0.284, 0.235, 0.356 µm respectively for specimen n° 23,24,25,26 (F82H). The Ra parameter was not specifically determined for each specimen before the test, anyway the values after the test can be compared to the ones of the representative specimen shown in Figure 3 (Eurofer 97; Ra = 0.308 µm) and in Figure 6 (F82H; Ra = 0.271 µm). It can be seen that the Ra values of the specimens after the test are essentially the same of the representative specimens, not exposed to the test, and surely well below the 3.0 µm set as starting surface requirement.

Even comparing the Rz values (which take into account, for each profiles, only the 5 highest peaks and the 5 deepest grooves), we can observe that the values are essentially unchanged by the execution of the erosion-corrosion test: 2.059, 2.225, 2.384, 2.403 µm respectively for specimen n° 2,3,4,5 vs (Eurofer 97) vs 2.289 (fresh specimen, Figure 3), and 2.230, 2.445, 1.786, 2.701 respectively for specimen n° 23,24,25,26 (F82H) vs 2.075 (fresh specimen, Figure 6).

On the whole, we can conclude that the surface profile was not affected, at least in an evident way, by the action of the flowing Lithium. This confirms the rather limited damage suffered by the specimens, as already evidenced by the very small mass diminutions.

2.4.5 SEM-EDS inspection of the specimens surfaces

This kind of inspection, as well as the following ones (respectively reported in section 2.4.6 and 2.4.7), has not been executed in ENEA Brasimone centre, but in Firenze, by the *INSTM Consortium* (*National Interuniversity Consortium of Materials Science and Technology*), with whom a collaboration has been activated.

Each specimen, once received from ENEA, has been cut through a cropper (*Remet MT micro*) in two pieces: the first one has been employed for the morphological and chemical analysis of the surface; the second one, after insertion into a resin and lapping, has been employed for the cross section investigations (section 2.4.6 and 2.4.7). Both fragments, after the cut, have been washed with demineralized water and dipped into acetone in a ultrasonic bath for 3 minutes; after being rinsed again with water and then acetone, they have been dried at room temperature.

It must be emphasized that, a part from the 8 specimens employed for the erosion-corrosion test, one additional fresh (unexposed to Lithium) specimen of each material has been inspected too by the *INSTM Consortium*, in order to perform a direct comparison of the analytical results, being them achieved with the same instrumentation and through the same sample preparation procedure.

The investigations reported in this section have been performed with an *Hitachi 2300* electron microscope (SEM) equipped with an X-ray spectrometer with wavelength dispersion (EDS) controlled by the *Noran System Six 3600* software.

Firstly, let's consider Eurofer 97 material, starting with a specimen not submitted to the erosion-corrosion action by the flowing liquid Lithium (fresh specimens, n°10).

Figure 13 shows, at different magnitudes (400x and 2000x), the surface of a representative region of this specimen: the scrapes of the mechanical manufacturing are clearly visible.

Figure 14 reports instead the EDS spectrum of this surface; Table 6 summarizes the values of the related semiquantitive analysis (average composition of a ~ 800 x 1000 μm^2 area).

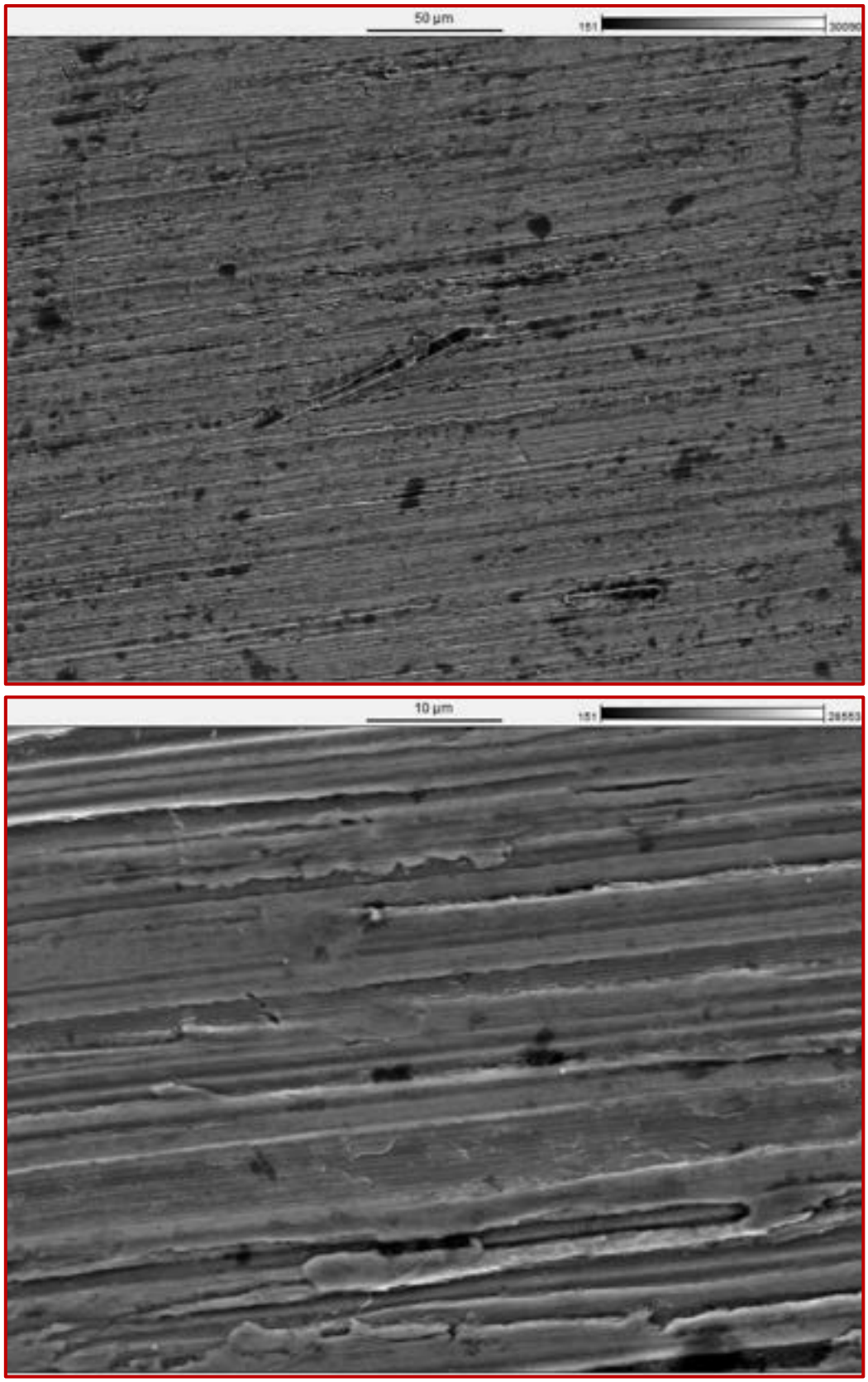

Figure 13: SEM images of specimen n°10 surface (secondary electrons) at different magnitudes. Scale bar above the image.

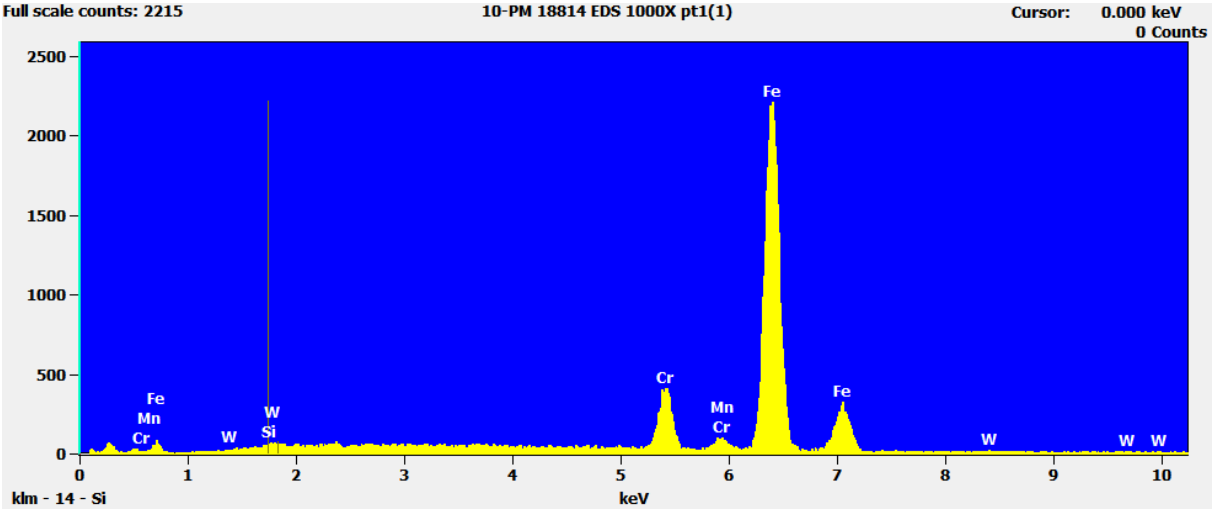

Figure 14: EDS spectrum obtained at specimen n°10 surface

Table 6: elements concentration at specimen n°10 surface from the EDS analysis.
Filter Fit, Chi² value: 4.254, Correct. Method: Proza (Phi-Rho-Z), Acc.Voltage: 20.0 kV, Take Off Angle: 90.0°.

Element	Weight conc. %	Atomic conc. %
Cr	8.5	9.1
Mn	0.8	0.9
Fe	88.9	89.5
W	1.8	0.5

Figure 15 shows instead, at different magnitudes, the surface of specimen n° 2, after the exposure to flowing Lithium.

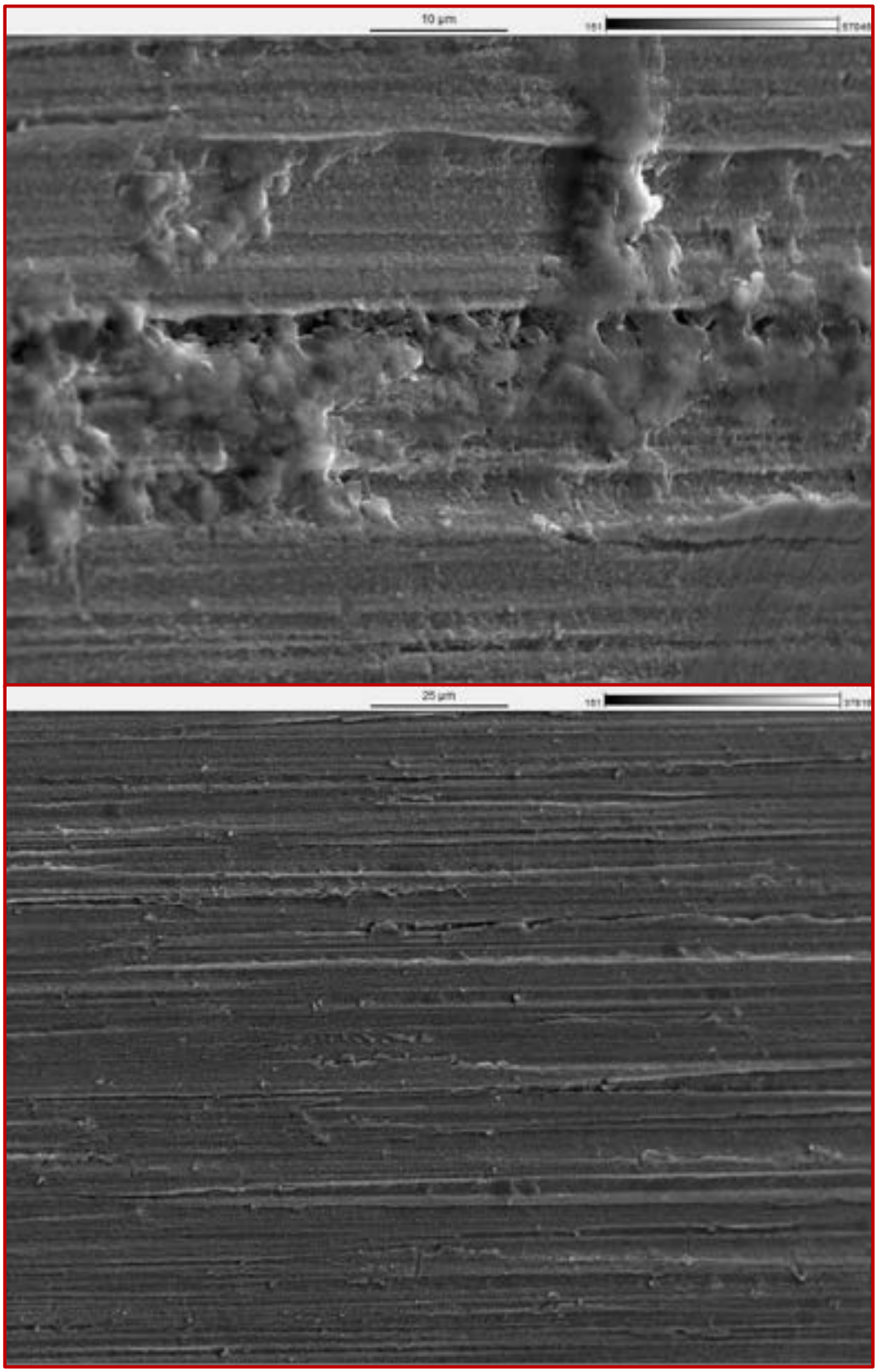

Figure 15: SEM images of specimen n°2 surface (secondary electrons) at different magnitudes. Scale bar above the image.

From the inspection of specimen n° 2 surface, no evident phenomenon of corrosion or erosion appears. All over the investigated surface are present instead the signs produced by the mechanical manufacturing, which precede the experimental test execution. Such signs are similar to the ones already observed on specimen n° 10 surface.

Figure 16 reports instead the EDS spectrum of specimen n° 2 surface; Table 7 summarizes the values of the related semiquantitive analysis (average composition of the investigated area). A small reduction of Cr and W, respect to the unexposed specimen, appears.

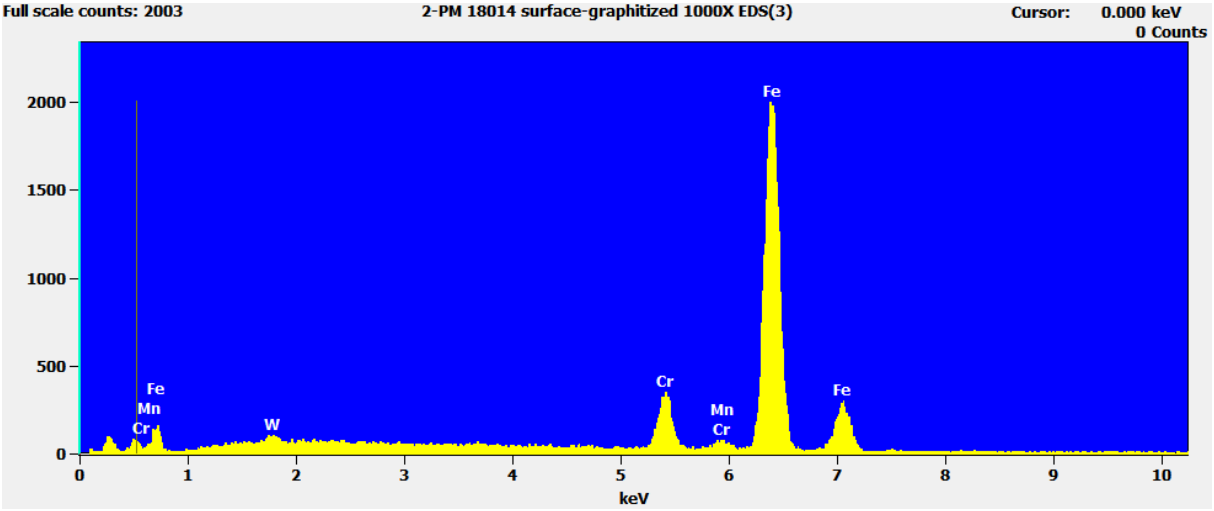

Figure 16: EDS spectrum obtained at specimen n°2 surface

Table 7: elements concentration at specimen n°2 surface from the EDS analysis.
Filter Fit, Chi² value: 4.254, Correct. Method: Proza (Phi-Rho-Z), Acc.Voltage: 20.0 kV, Take Off Angle: 90.0°.

Element	Weight conc. %	Atomic conc. %
Cr	7.8	8.4
Mn	0.4	0.4
Fe	91.0	91.0
W	0.8	0.3

Figure 17 shows, at different magnitudes, the surface of specimen n° 3, after the exposure to flowing Lithium.

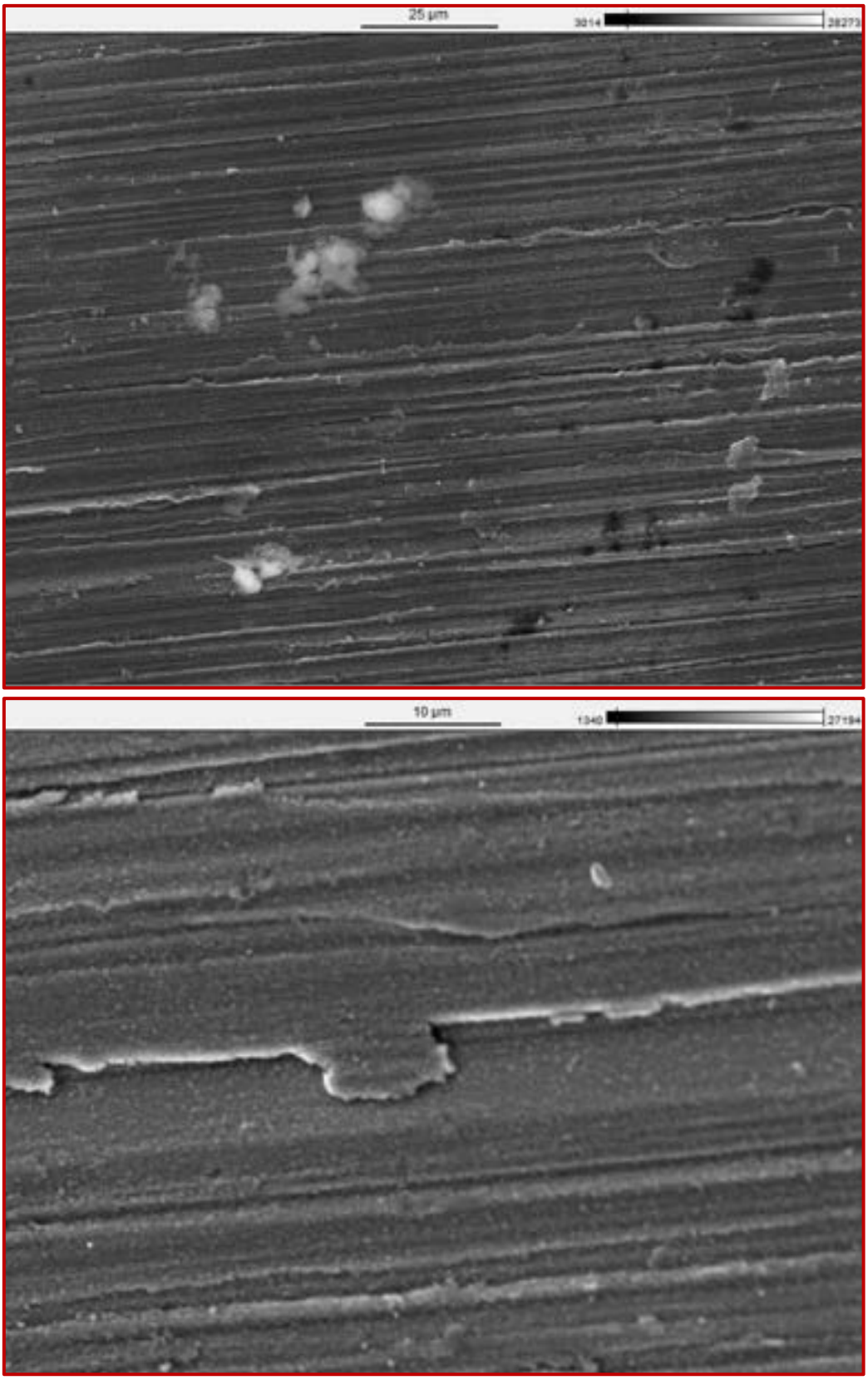

Figure 17: SEM images of specimen n° 3 surface (secondary electrons) at different magnitudes. Scale bar above the image.

Also for this specimen, the observed morphology is a consequence of the mechanical manufacturing executed before the erosion-corrosion test.

Figure 18 reports instead the EDS spectrum of specimen n° 3 surface; Table 8 summarizes the values of the related semiquantitive analysis (average composition of the investigated area). A small decrease of Cr concentration, respect to the unexposed specimen, is visible again.

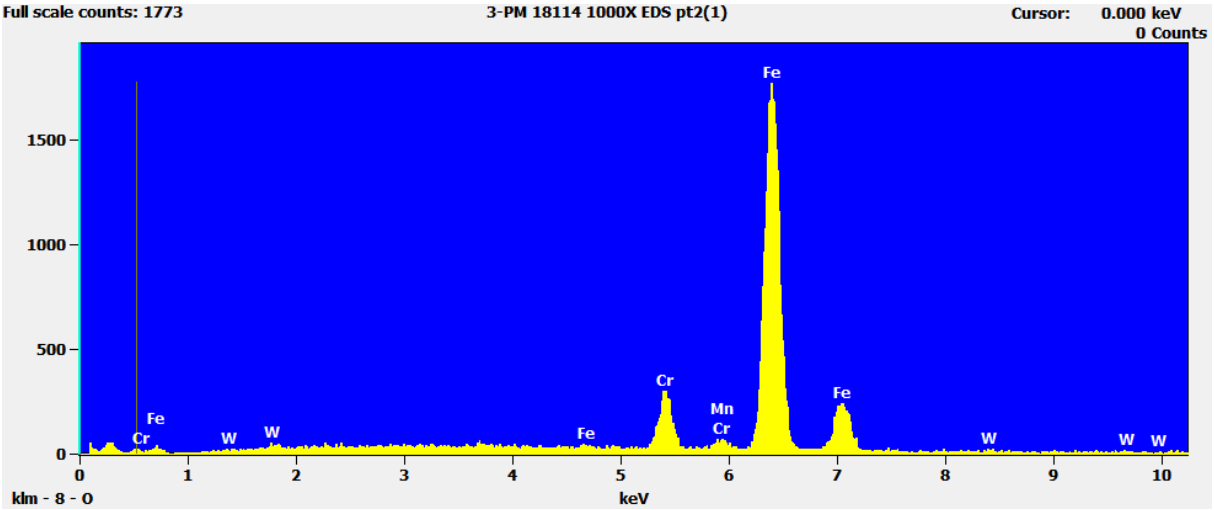

Figure 18: EDS spectrum obtained at specimen n°3 surface

Table 8: elements concentration at specimen n°3 surface from the EDS analysis.
Filter Fit, Chi² value: 4.254, Correct. Method: Proza (Phi-Rho-Z), Acc.Voltage: 20.0 kV, Take Off Angle: 90.0°.

Element	Weight conc. %	Atomic conc. %
Cr	7.2	7.8
Mn	0.4	0.4
Fe	90.9	91.3
W	1.5	0.5

Figure 19 shows, at different magnitudes, the surface of specimen n° 4, after the exposure to flowing Lithium.

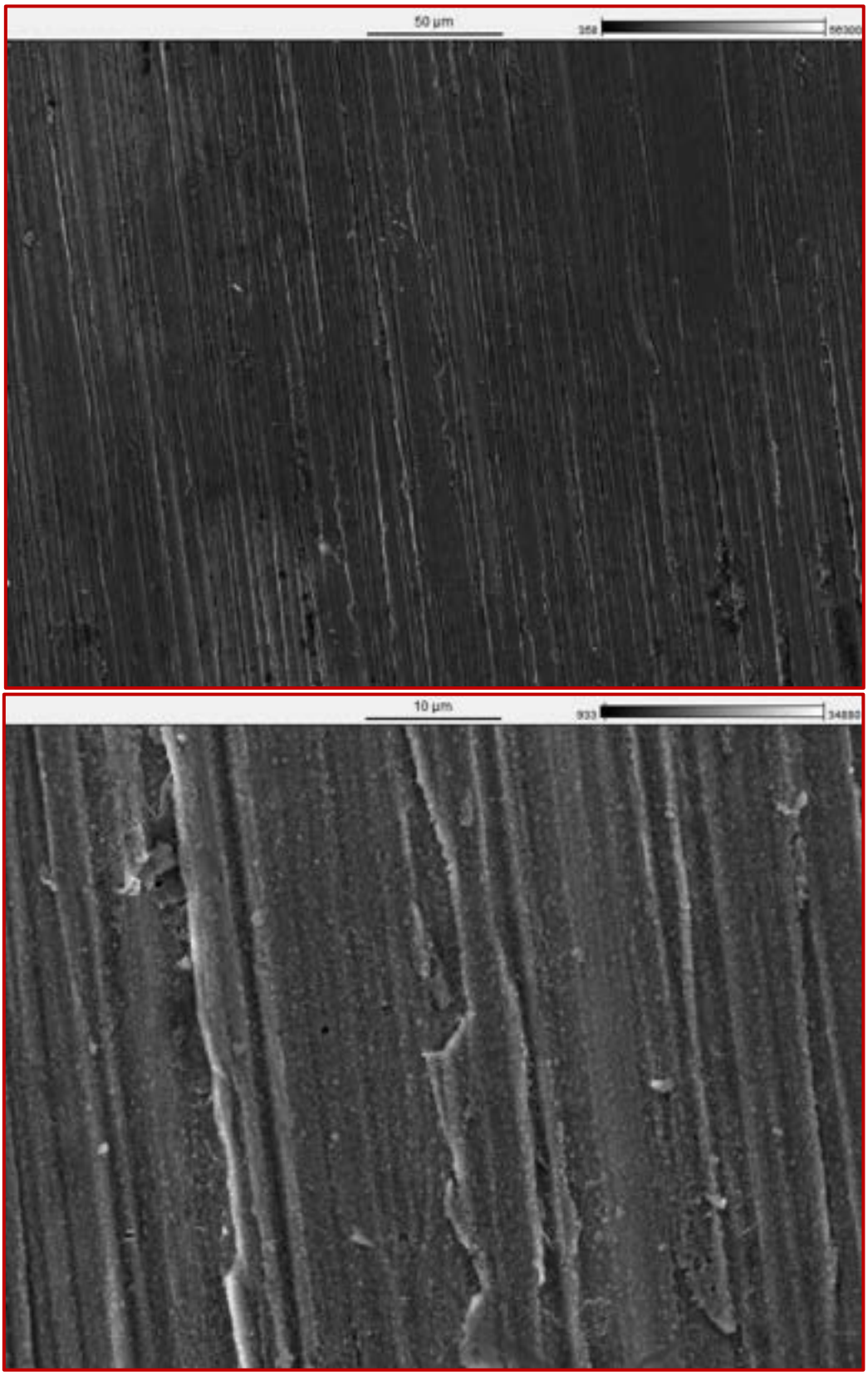

Figure 19: SEM images of specimen n°4 surface (secondary electrons) at different magnitudes. Scale bar above the image.

The same considerations made for specimen n°2 and n°3 hold also for specimen n°4.

Figure 20 reports the EDS spectrum of specimen n° 4 surface; Table 9 summarizes the values of the related semiquantitive analysis (average composition of the investigated area). Also in this case there seems to be a minimal diminution of Cr concentration at the surface, respect to the unexposed specimen.

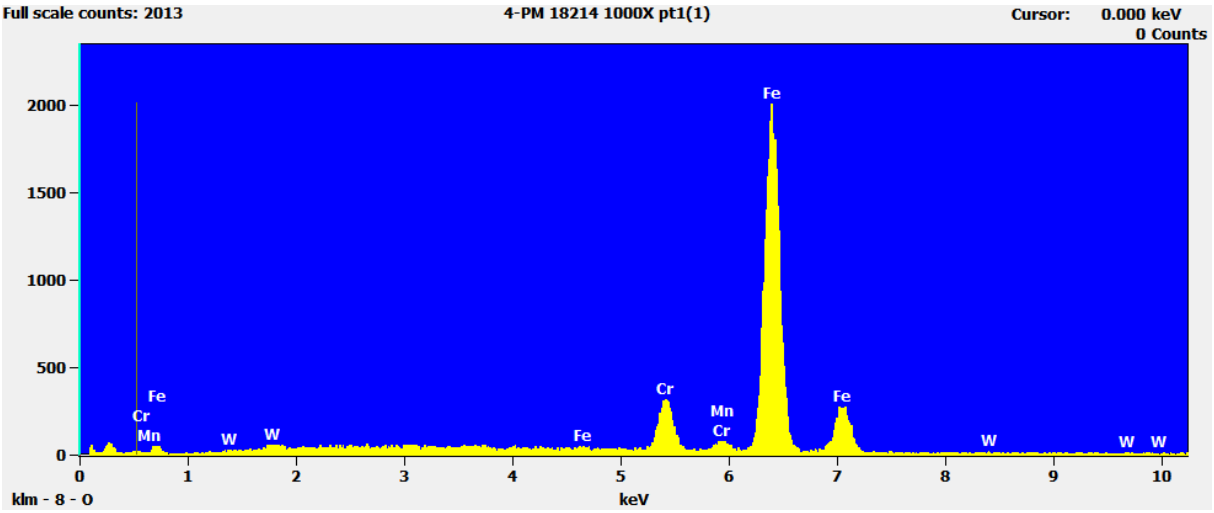

Figure 20: EDS spectrum obtained at specimen n°4 surface

Table 9: elements concentration at specimen n°4 surface from the EDS analysis.
Filter Fit, Chi² value: 4.254, Correct. Method: Proza (Phi-Rho-Z), Acc.Voltage: 20.0 kV, Take Off Angle: 90.0°.

Element	Weight conc. %	Atomic conc. %
Cr	7.6	8.2
Mn	0.8	0.8
Fe	90.3	90.6
W	1.3	0.4

The surface of specimen n°5, at different magnitudes, is instead shown in Figure 21. Apart from the already observed signs of manufacturing, in this sample dark spots and white not conductive corpuscles (high resolution part of Figure 21) are evident. In both cases, the punctual EDS analysis of these specific regions has not indicated meaningful differences respect to the average surface composition (reported in Figure 22 and Table 10). It's possible that these features have organic nature (Carbon and Oxygen are not quantifiable with this kind of analysis) and are due to small contamination after the erosion-corrosion test.

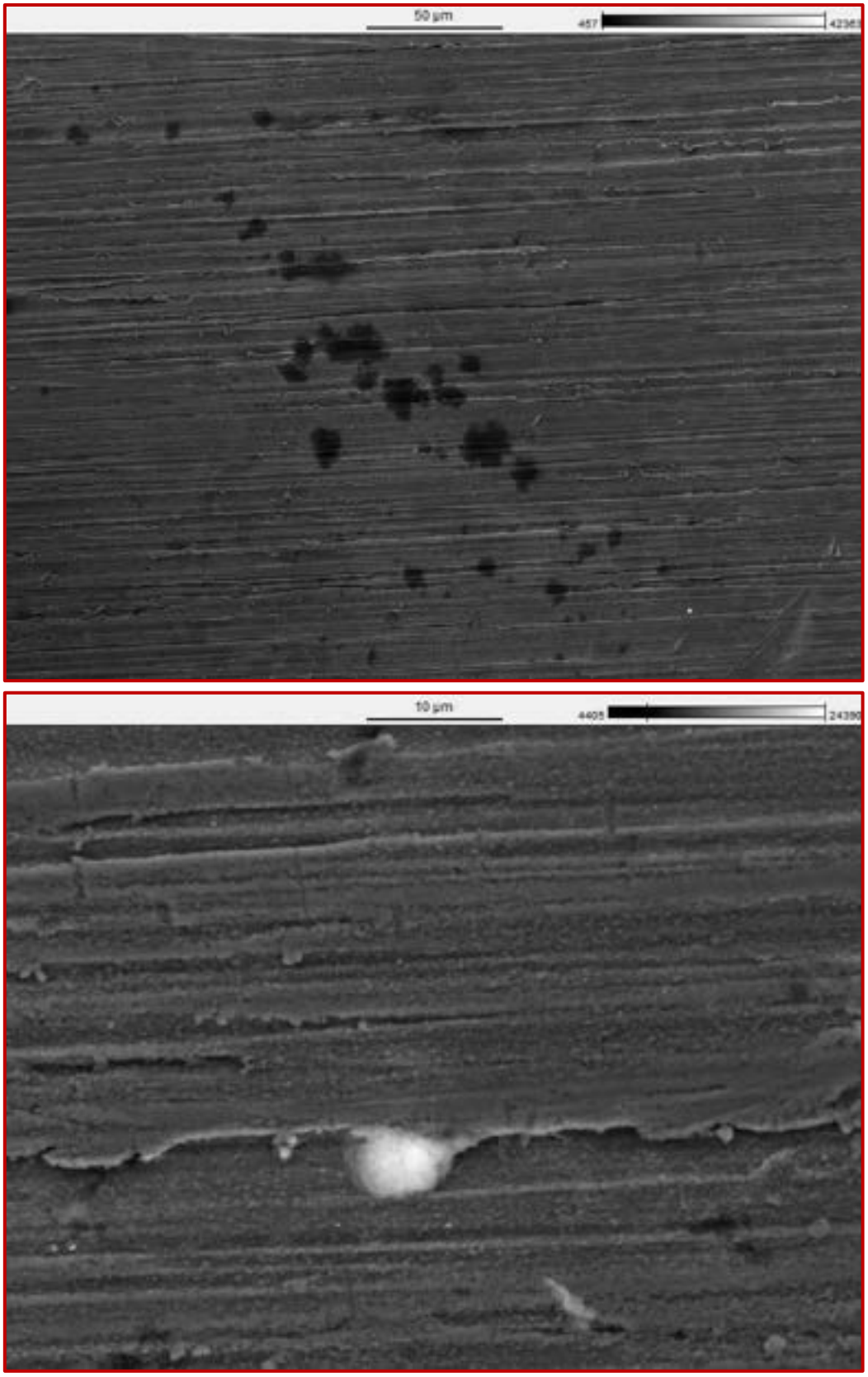

Figure 21: SEM images of specimen n°5 surface (secondary electrons) at different magnitudes. Scale bar above the image.

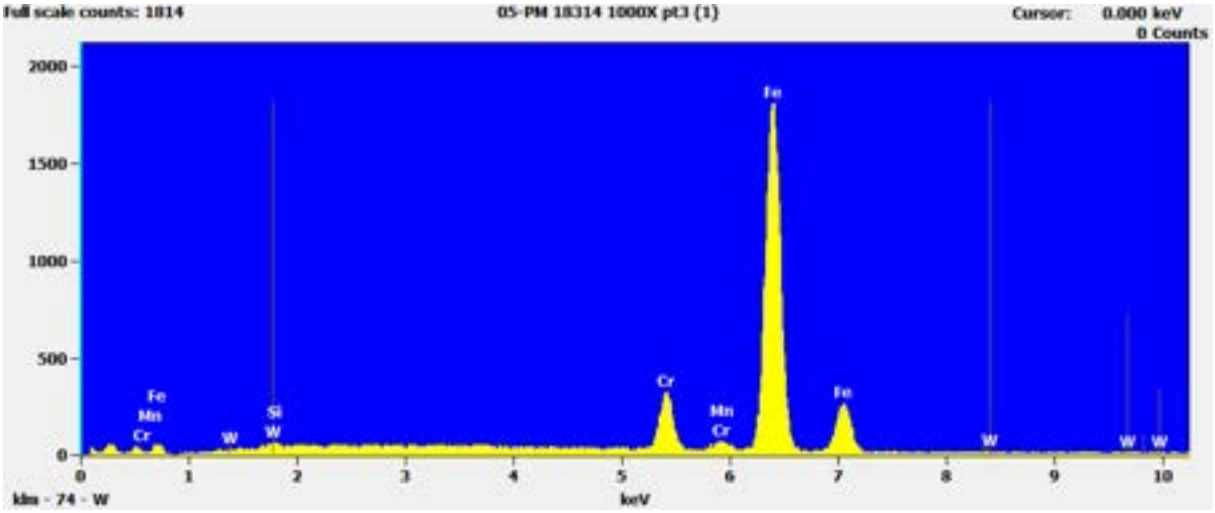

Figure 22: EDS spectrum obtained at specimen n°5 surface

Table 10: elements concentration at specimen n°5 surface from the EDS analysis.
Filter Fit, Chi² value: 4.254, Correct. Method: Proza (Phi-Rho-Z), Acc.Voltage: 20.0 kV, Take Off Angle: 90.0°.

Element	Weight conc. %	Atomic conc. %
Si	0.1	0.2
Cr	7.6	8.2
Mn	0.5	0.5
Fe	91.3	91.0
W	0.4	0.13

A small decrease of Cr and W concentration, respect to the surface of the unexposed specimen, is evident.

Now, let's look at the F82H specimens. Let's start with the one not submitted to the erosion-corrosion action by the flowing liquid Lithium (fresh specimens, n° 31).

Figure 23 shows, at different magnitudes, the surface of a representative region of this specimen. As already observed for the Eurofer 97 specimens, also here the sample surface is characterized by the presence of signs due to the mechanical manufacturing, while surface alterations due to erosion-corrosion by Lithium are (of course) absent.

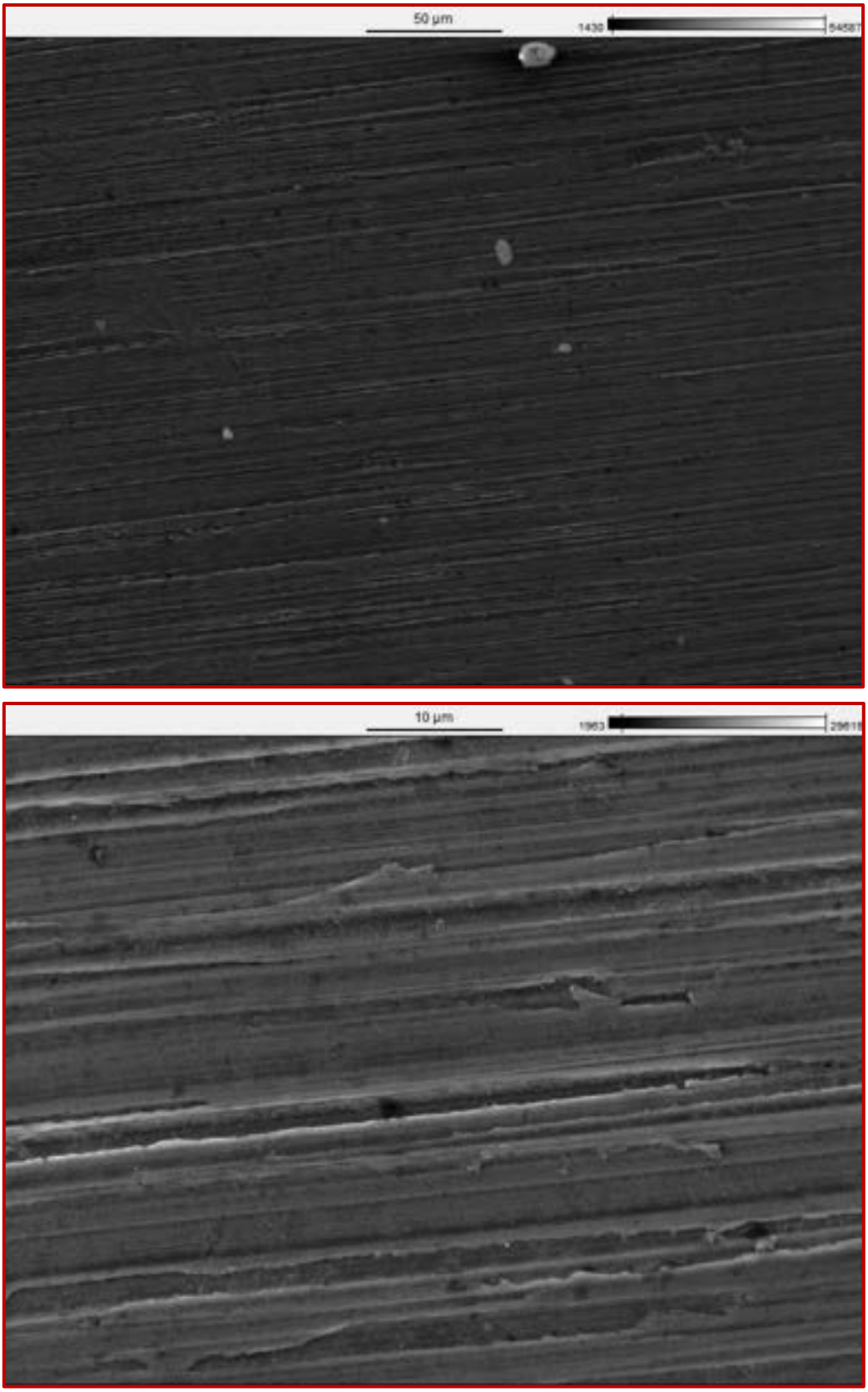

Figure 23: SEM images of specimen n° 31 surface (secondary electrons) at different magnitudes. Scale bar above the image.

Figure 24 reports the EDS spectrum of specimen n° 31 surface; Table 11 summarizes the values of the related semiquantitive analysis (average composition of the investigated area).

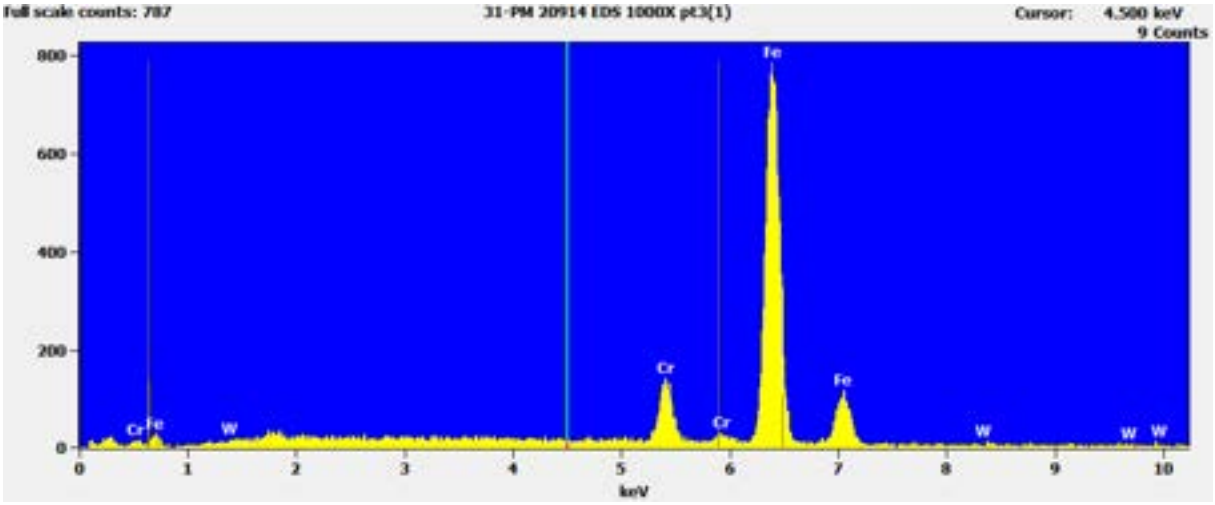

Figure 24: EDS spectrum obtained at specimen n°31 surface

Table 11: elements concentration at specimen n°31 surface from the EDS analysis.
Filter Fit, Chi² value: 4.254, Correct. Method: Proza (Phi-Rho-Z), Acc.Voltage: 20.0 kV, Take Off Angle: 90.0°.

Element	Weight conc. %	Atomic conc. %
Cr	8.0	8.7
Fe	88.5	90.2
W	3.5	1.1

One of the white corpuscles sporadically present on the surface was anyway investigated in depth, trying to understand its nature. Figure 25 is an enlargement of the top image of Figure 23, centered on one of these white bodies. Two EDS spectrum were performed, the first investigating the position indicated by '1' in Figure 25 (surface matrix), the second the position indicated by '2' (white anomaly), to compare the concentrations of the elements in the different locations.

Figure 26 contemporary shows the two EDS spectra (position '1': red plot; position '2': yellow plot), pointing out that the white particle is characterized by a significant concentration of O, Na and mostly C and Ca (maybe some residue of alkaline carbonate). Since specimen n°31 was not exposed to Lithium, surely the presence of the just mentioned elements must be ascribed to the sample handling and its treatment before the execution of the analysis. In any case this conclusion allows to exclude, also for the really exposed specimens, that similar surface anomalies are somehow consequence of the action exerted by the liquid Lithium.

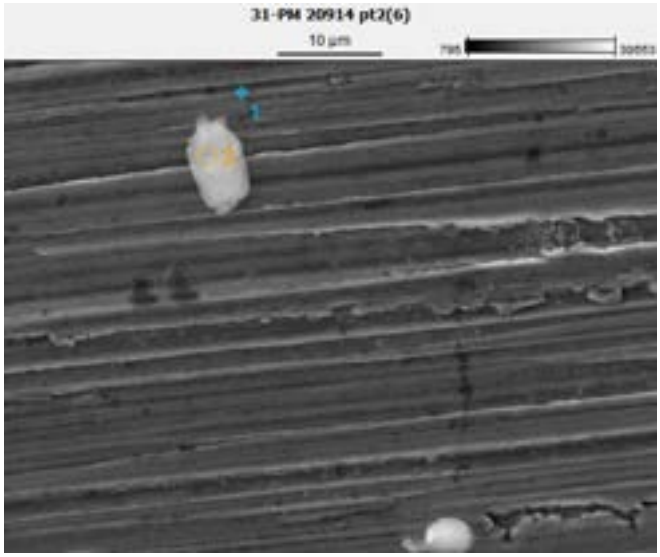

Figure 25: enlargement of the top image of Figure 23, centred on one of the unknown white bodies (secondary electrons). Scale bar above the image.

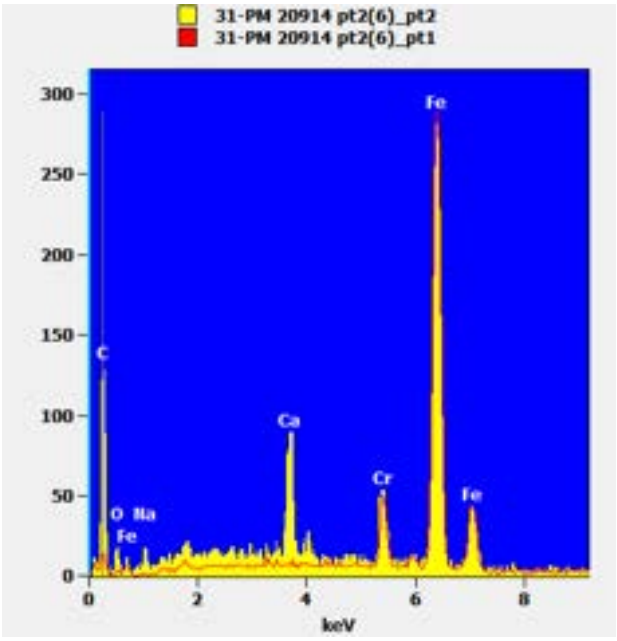

Figure 26: EDS spectrum obtained in correspondence of position '1' and position '2' on the surface of specimen n° 31; relative positions are indicated in Figure 25.

The surface of specimen n°23 is shown, at different magnitudes, in Figure 27. It appears substantially identical to the reference one (specimen n°31).

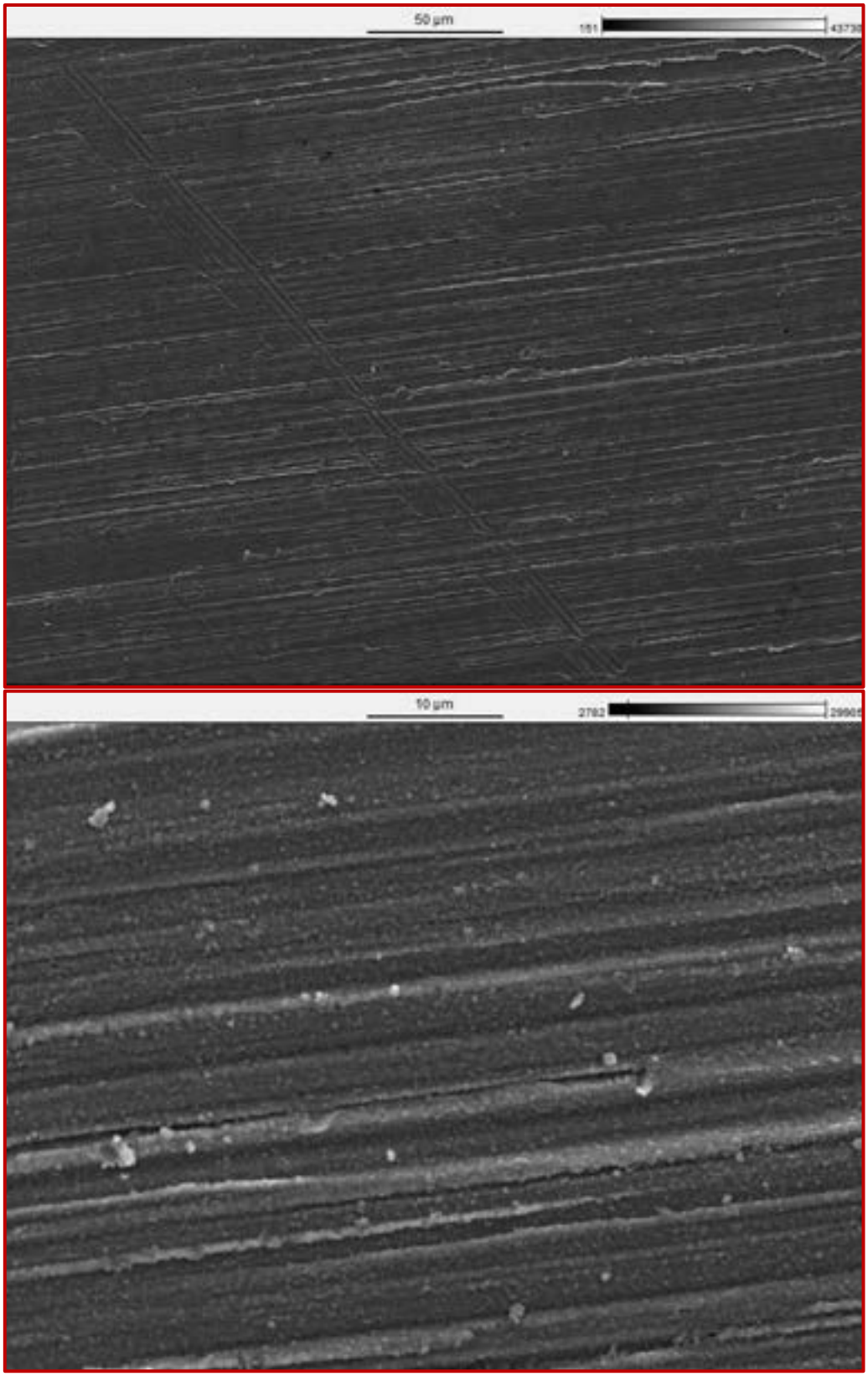

Figure 27: SEM images of specimen n° 23 surface (secondary electrons) at different magnitudes. Scale bar above the image.

Figure 28 reports instead the EDS spectrum of specimen n° 23 surface; Table 12 summarizes the values of the related semiquantitive analysis (average composition of the investigated area).

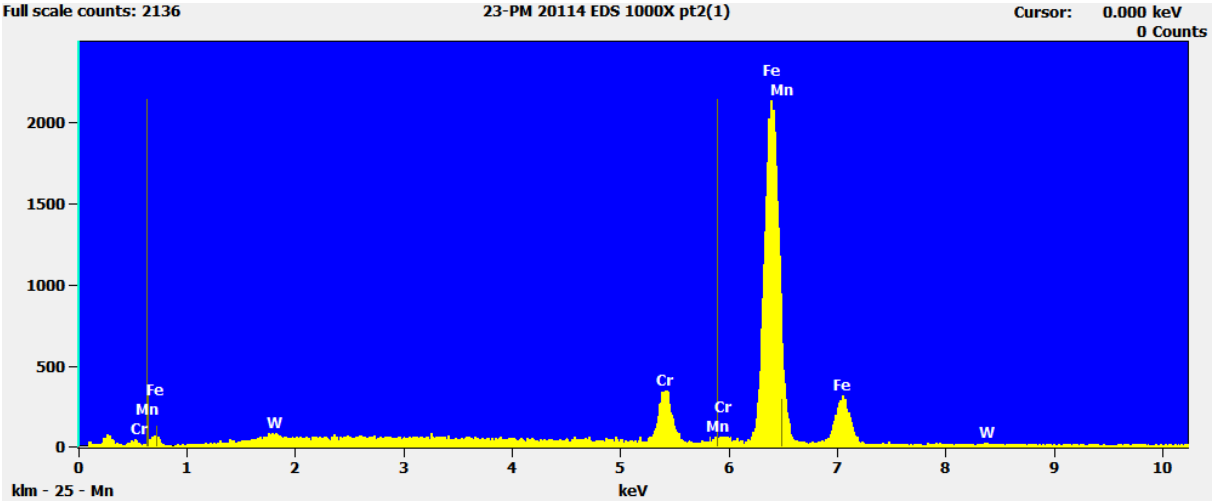

Figure 28: EDS spectrum obtained at specimen n°23 surface

Table 12: elements concentration at specimen n°23 surface from the EDS analysis.
Filter Fit, Chi² value: 4.254, Correct. Method: Proza (Phi-Rho-Z), Acc.Voltage: 20.0 kV, Take Off Angle: 90.0°.

Element	Weight conc. %	Atomic conc. %
Cr	6.8	7.4
Mn	-	-
Fe	90.9	91.9
W	2.3	0.7

Comparing the above values with the ones in Table 11, a small decrease of Cr concentration can be noted, as well as W one.

Figure 29 shows, at different magnitudes, the surface of specimen n°24. No substantial alteration of the morphology appears respect to the starting conditions (specimen n°31).

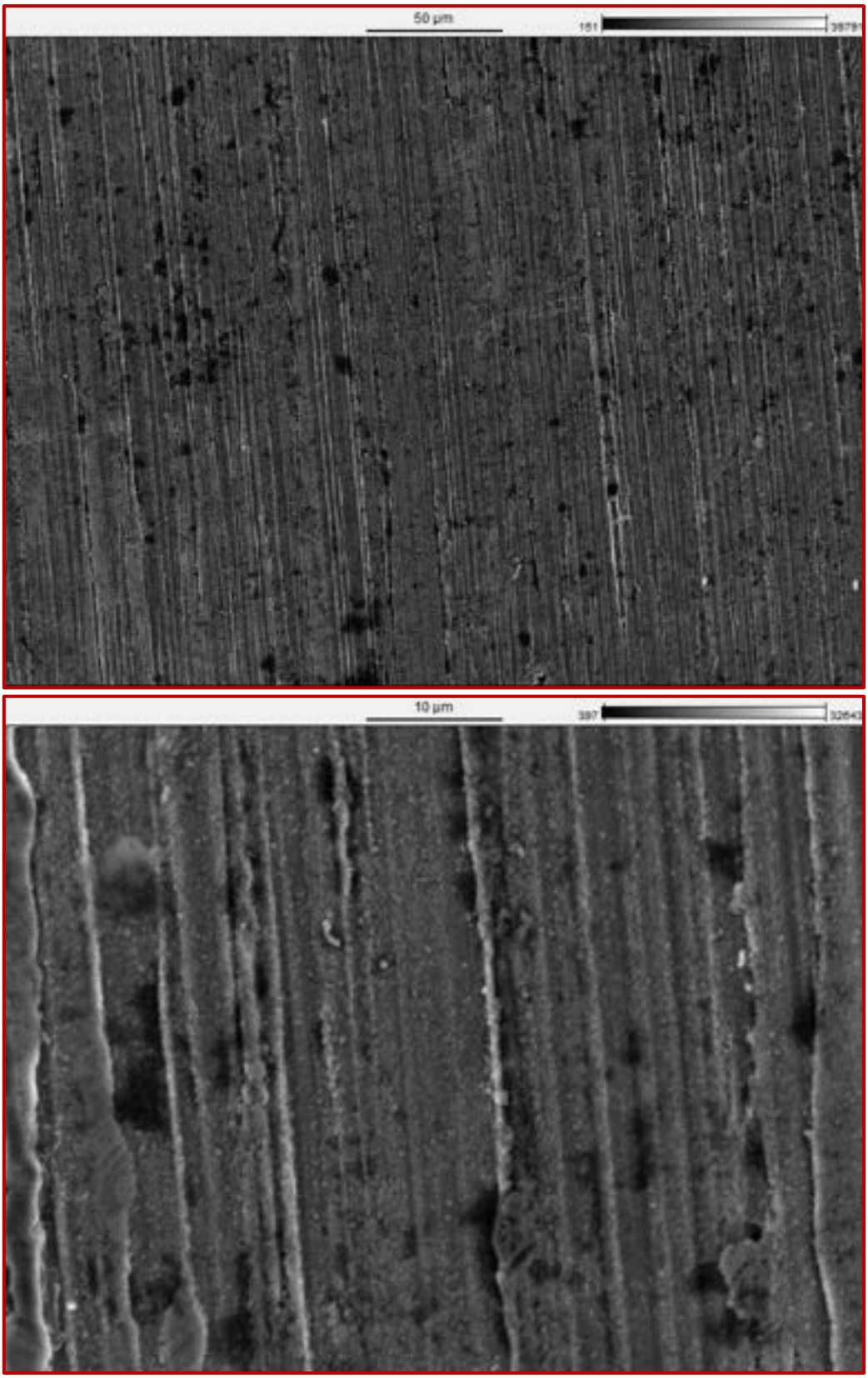

Figure 29: SEM images of specimen n° 24 surface (secondary electrons) at different magnitudes. Scale bar above the image.

Figure 30 reports instead the EDS spectrum of specimen no 24 surface; Table 13 summarizes the values of the related semiquantitive analysis (average composition of the investigated area).

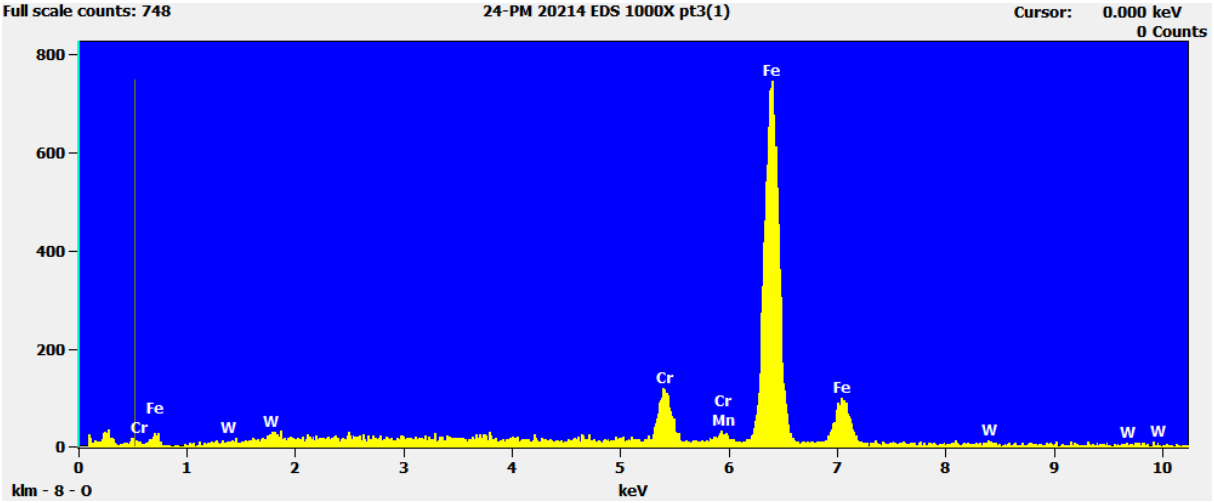

Figure 30: EDS spectrum obtained at specimen n°24 surface

Table 13: elements concentration at specimen n°24 surface from the EDS analysis.
Filter Fit, Chi² value: 4.254, Correct. Method: Proza (Phi-Rho-Z), Acc.Voltage: 20.0 kV, Take Off Angle: 90.0°.

Element	Weight conc. %	Atomic conc. %
Cr	7.4	8.1
Mn	0.4	0.4
Fe	88.9	90.5
W	3.3	1.0

Comparing the above values with the ones in Table 11, a small decrease of Cr concentration can be noted.

Figure 31 shows, at different magnitudes, the surface of specimen n°25. No substantial alteration of the morphology appears respect to the unexposed specimen (n°31).

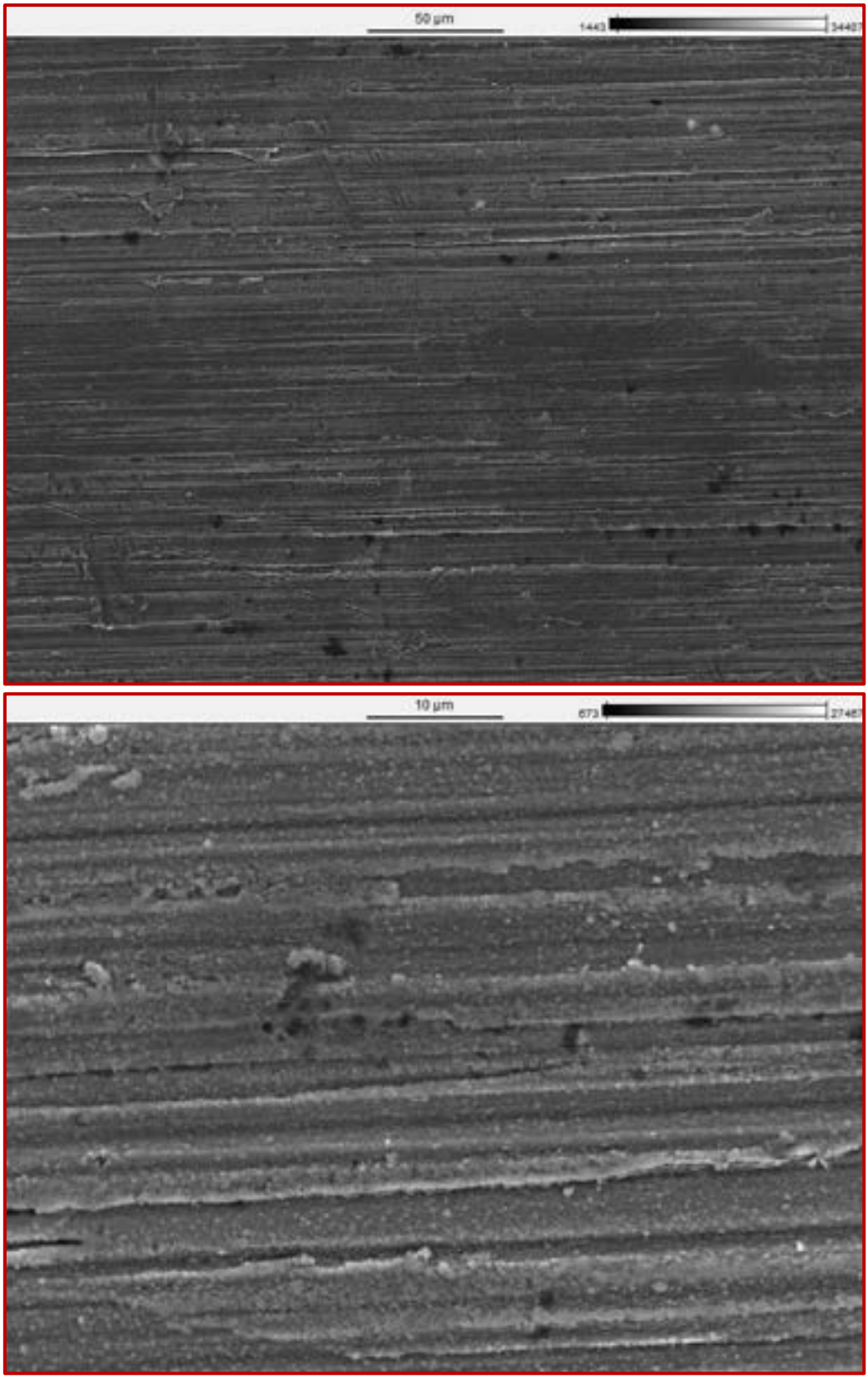

Figure 31: SEM images of specimen n° 25 surface (secondary electrons) at different magnitudes. Scale bar above the image.

Figure 32 reports instead the EDS spectrum of specimen no 25 surface; Table 14 summarizes the values of the related semiquantitive analysis (average composition of the investigated area).

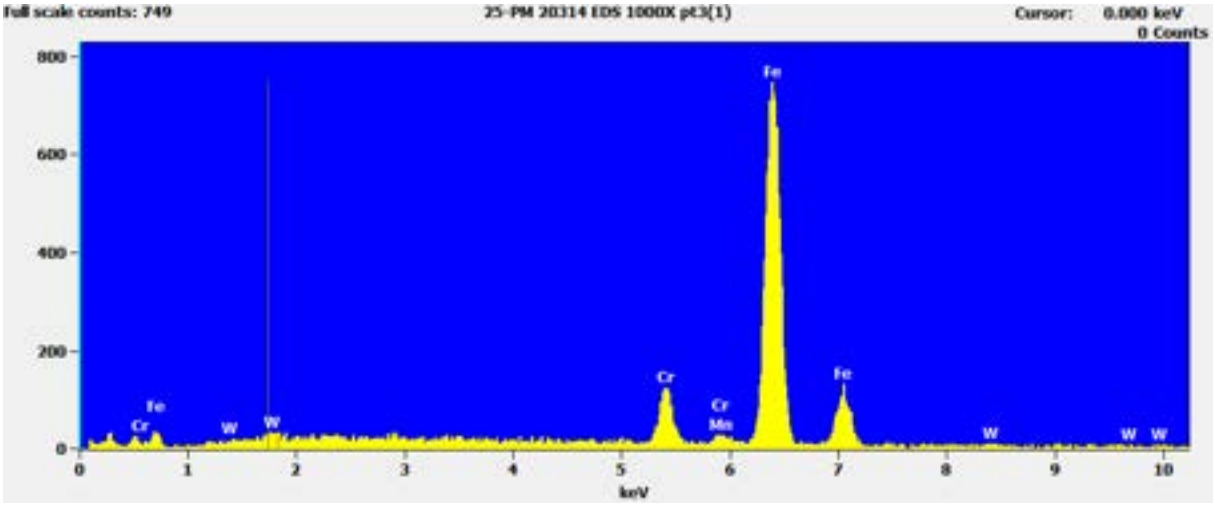

Figure 32: EDS spectrum obtained at specimen n°25 surface

Table 14: elements concentration at specimen n°25 surface from the EDS analysis.
Filter Fit, Chi² value: 4.254, Correct. Method: Proza (Phi-Rho-Z), Acc.Voltage: 20.0 kV, Take Off Angle: 90.0°.

Element	Weight conc. %	Atomic conc. %
Cr	6.9	7.5
Mn	0.4	0.4
Fe	90.1	91.3
W	2.6	0.8

Comparing the above values with the ones in Table 11, a small decrease of Cr and W concentration can be noted.

Figure 33 shows, at different magnitudes, the surface of specimen n°26.

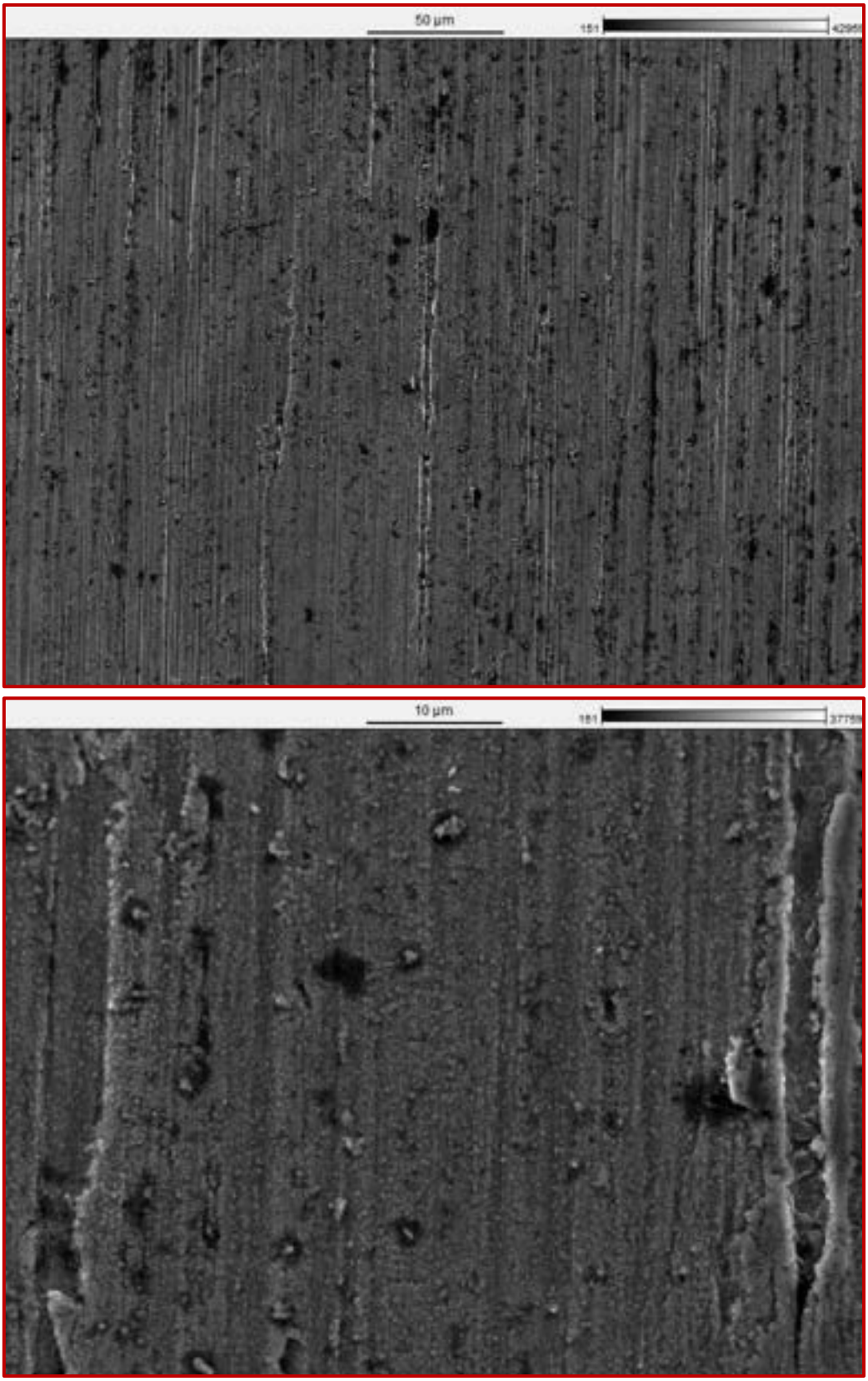

Figure 33: SEM images of specimen n° 26 surface (secondary electrons) at different magnitudes. Scale bar above the image.

Figure 34 reports instead the EDS spectrum of specimen n° 26 surface; Table 15 summarizes the values of the related semiquantitive analysis (average composition of the investigated area).

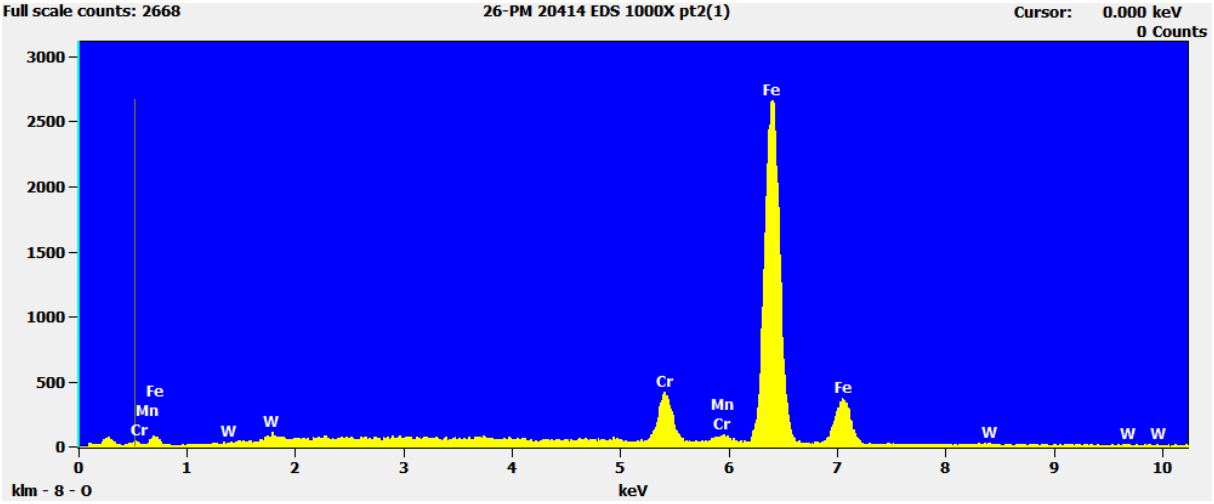

Figure 34: EDS spectrum obtained at specimen n°26 surface

Table 15: elements concentration at specimen n°26 surface from the EDS analysis.
Filter Fit, Chi² value: 4.254, Correct. Method: Proza (Phi-Rho-Z), Acc.Voltage: 20.0 kV, Take Off Angle: 90.0°.

Element	Weight conc. %	Atomic conc. %
Cr	7.0	7.6
Mn	0.2	0.2
Fe	90.7	91.6
W	2.1	0.7

Comparing the above values with the ones in Table 11, a small decrease of Cr and W concentration can be noted.

Looking at Figure 33, we don't note morphological alterations of the surface respect to the unexposed one (specimen n°31). Anyway, many small black spots can be seen. In order to better investigate the nature of this black spots, two additional EDS spectrum were performed, the first investigating the position indicated by '1' (dark region) in Figure 35 (higher magnitude image of surface specimen), the second investigating the position indicated by '2' (surface matrix), to compare the concentrations of the elements in the two different locations.

Figure 36 contemporary shows the two EDS spectra (position '1': yellow plot; position '2': red plot). The two spectra are almost identical: the only difference is the slightly higher concentration of Oxygen in the dark region (position '1'), which remains anyway small and not quantifiable with this technique.

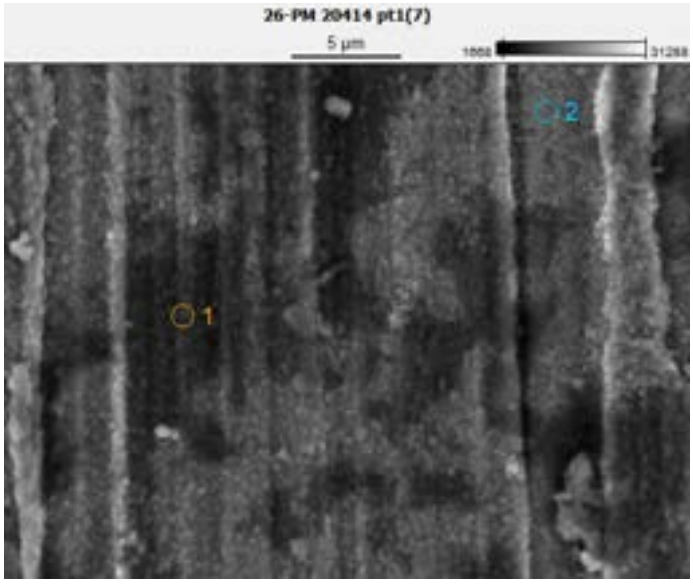

Figure 35: high magnitude image of specimen n°26 surface, highlighting a darker region ('1') and a 'regular' one ('2') (secondary electrons). Scale bar above the image.

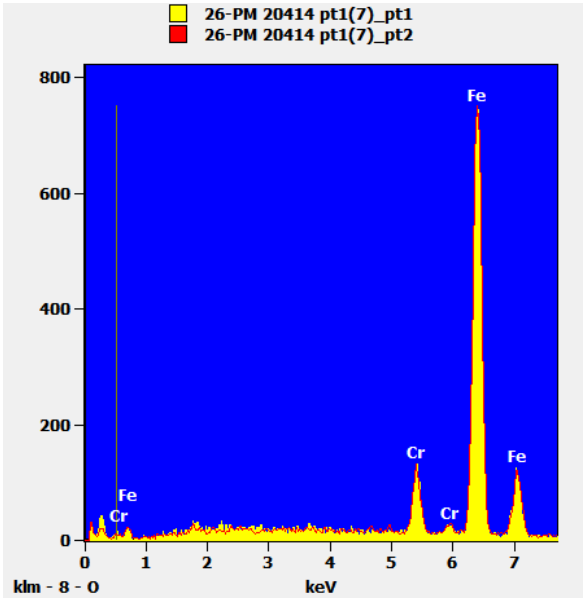

Figure 36: EDS spectrum obtained in correspondence of position '1' and position '2' on the surface of specimen n°26; relative position is indicated in Figure 35.

Such an Oxygen increase in position '1' might be viewed a consequence of some oxidation process. This process could have occurred during the erosion-corrosion test (by the Oxygen solved in Lithium ?), but it is more likely to have occurred during the cleaning of the specimen, when it was kept for about 45' in boiling water. In any case, the entity of the phenomenon is very small.

Finally, Table 16 summarizes all the already reported specimens compositions, as determined by the EDS analysis.

Table 16: measured elements concentrations at the surfaces of the specimens after the test (wt %)

Material	EU 97	EU 97	EU 97	EU 97	EU 97	F82H	F82H	F82H	F82H	F82H
Sample ID	10	2	3	4	5	31	23	24	25	26
Cr	8.5	7.8	7.2	7.6	7.6	8.0	6.8	7.4	6.9	7.0
Mn	0.8	0.4	0.4	0.8	0.5	-	-	0.4	0.4	0.2
Fe	88.9	91.0	90.9	90.3	91.3	88.5	90.9	88.9	90.1	90.7
W	1.8	0.8	1.5	1.3	0.4	3.5	2.3	3.3	2.6	2.1
ΔW	***unexposed***	**-1.0**	**-0.3**	**-0.5**	**-1.4**	***unexposed***	**-1.2**	**-0.2**	**-0.9**	**-1.4**
ΔCr	***unexposed***	**-0.7**	**-1.3**	**-0.9**	**-0.9**	***unexposed***	**-1.2**	**-0.6**	**-1.1**	**-1.0**

The table doesn't show large concentration variations as a consequence of the test, considering the ± ~ 0.5 wt % uncertainty in the reported values. Anyway, it seems that maybe some W diminution occurred and almost surely this occurred in the case of Cr.

For W not all the analyzed specimens are characterized by a significant concentration decrease. Specimen n° 3 and n° 24 are in fact characterized by only ~ 0.2-0.3 wt % W decrease, which doesn't necessarily indicate a real composition variation. Moreover, almost all the detected W concentrations are high respect to the theoretical composition reported in the materials supplier datasheets (1.06% for Eurofer 97 – Table 2 – and 1.98% for F82H – Table 3), so we can actually think that the unexposed specimens W concentration was slightly overestimated by the EDS analysis, this way increasing a little the calculated concentration diminutions in the exposed specimens.

In the case of Chromium the minimum concentration diminution is instead 0.6% and the average diminution (considering all the specimens) is ~ 1%. Considering moreover that all the Cr values in Table 16 are also smaller than in the material supplier datasheets (8.95% for Eurofer 97 – Table 2- and 7.87% for F82H – Table 3), we can conclude that the observed Chromium depletion is real.

Next erosion-corrosion tests, involving the same materials but for longer durations, are called to confirm, eventually in a more pronounced way, this phenomenon.

2.4.6 SEM-EDS inspection of the specimens cross section

As anticipated in section 2.4.5 introductive part, also the specimen cross section has been investigated, in order to detect possible corrosion phenomena (like pitting) also below the exposed surface. To prepare the sample, the fragment of specimen obtained after the cut has been inserted into a graphite conductive resin (*Konductomet®, Buehler*) and polished with abrasive papers (from 180 to 2500 grit) and diamond pastes (9, 6 and 3 µm, Metadi suspension, Buehler). Both morphological inspections (SEM) and chemical concentration profiles along the depth (EDS) have been then executed.

Again, let's consider first Eurofer 97 material, starting with the specimen not submitted to the erosion-corrosion action by the flowing liquid Lithium (fresh specimens, n°10).

Figure 37 shows on the left a SEM representative image of specimen n° 10 section, with the red Chromium concentration profile overlapped, as determined by the EDS analysis; the dark region is due to the supporting resin. On the right side of Figure 37 is instead reported a graph showing the profiles of both Chromium and Iron elements, where y-axis is the weight % concentration, while x-axis indicates the distance from the surface (the surface position is on the right boundary of the graph; x = 0 corresponds instead to the starting point of the yellow arrow). Many equidistant points have been considered for the EDS analysis, in the arrow direction, from a starting a depth of ~ 35 µm below the surface. The profiles have been constructed by joining the calculated points with straight lines. The absolute values of both Cr and Fe are probably a bit higher than the real one, because other minority elements have been excluded from the calculation, hence the software calculates the Cr and Fe concentration values in a way their sum is 100%: what is important is the qualitative trend of the profiles.

From the observation of the Figure, it is possible to note that the internal specimen structure is in good condition, with only some sign due to the cut and preparation of the sample, but no erosion-corrosion damage: this is of course what expected, since specimen n° 10 is an unexposed specimen. The concentration profiles indicate a substantial constancy of values, with perhaps only a minimal decrease of Cr concentration in the first microns below the surface.

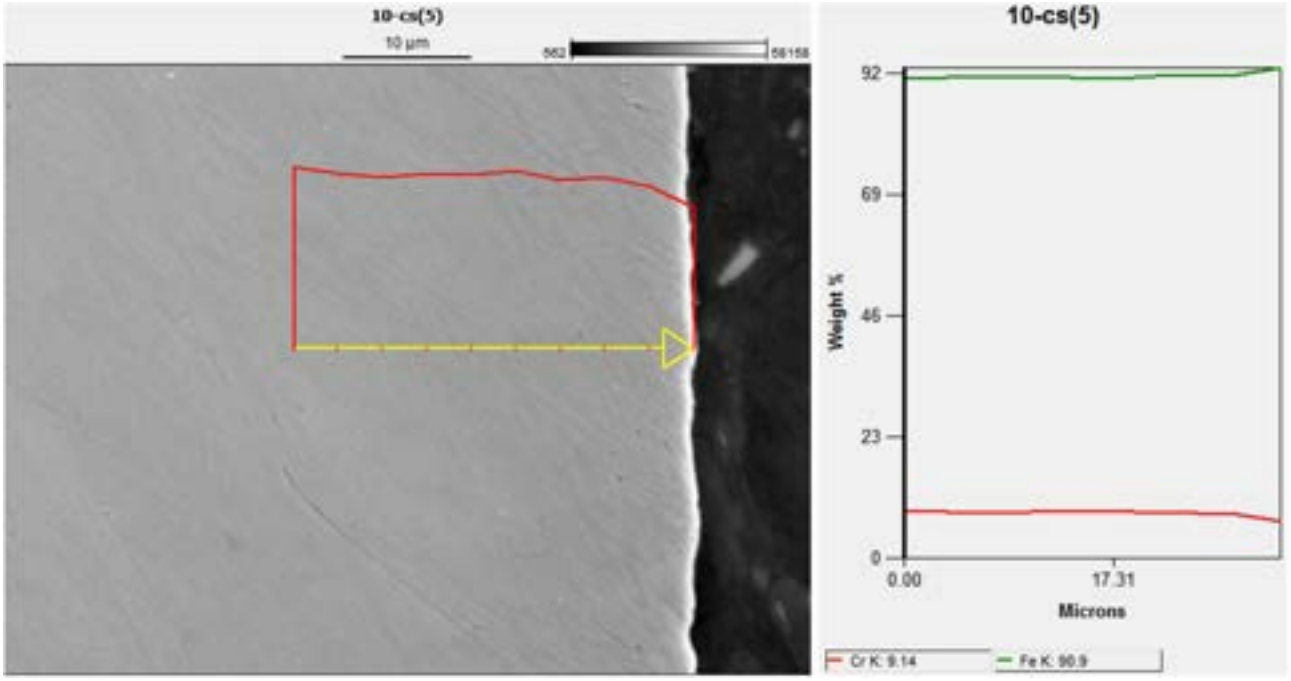

Figure 37: left: SEM image and Cr concentration profile (EDS) of specimen n°10 cross section; right: Cr (red) and Fe (green) concentration profiles along the specimen section.

Let's consider now the Eurofer 97 specimens tested in Lifus 6 plant. Figure 38 shows on the left a SEM representative image of specimen n° 2 section, with the red Chromium concentration profile overlapped, as determined by the EDS analysis; on the right side is instead reported a graph showing the profiles of both Chromium and Iron elements. The graph meaning and details are the same already described for Figure 37. A part from the signs due to the cut and preparation of the sample, no erosion-corrosion damage is shown by the SEM image: the appearance of the specimens section is quite similar to the one in Figure 37. For what concerns the concentration profiles, they are rather flat (small oscillations can be related to uncertainty in the EDS analysis result), even if in the case of Cr the concentration values seem to be slightly smaller than in specimen n° 10.

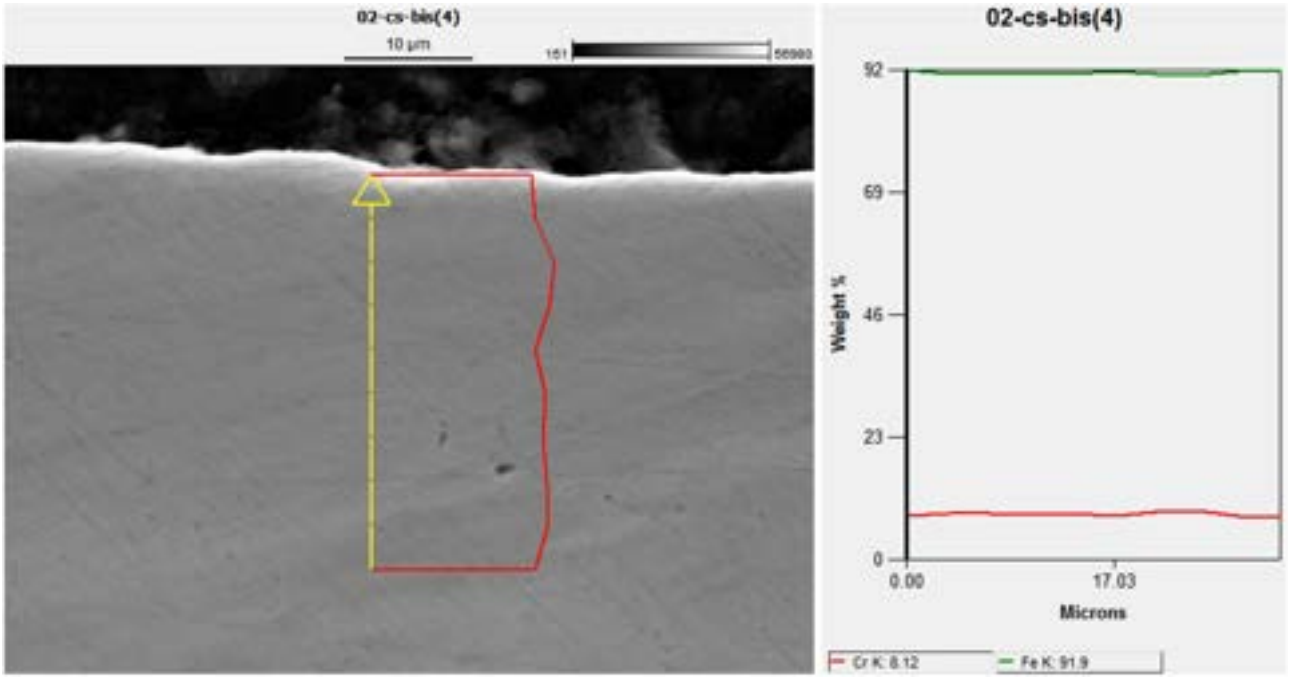

Figure 38: left: SEM image and Cr concentration profile (EDS) of specimen n°2 cross section; right: Cr (red) and Fe (green) concentration profiles along the specimen section.

Figure 39 shows on the left a SEM representative image of specimen n° 3 section, with the red Chromium concentration profile overlapped, as determined by the EDS analysis; on the right side is instead reported a graph showing the profiles of both Chromium and Iron elements. The graph meaning and details are the same already described for Figure 37. No internal morphological damage is evident; the concentration profiles are rather flat, a part from some small oscillations due to the uncertainty in the EDS analysis result.

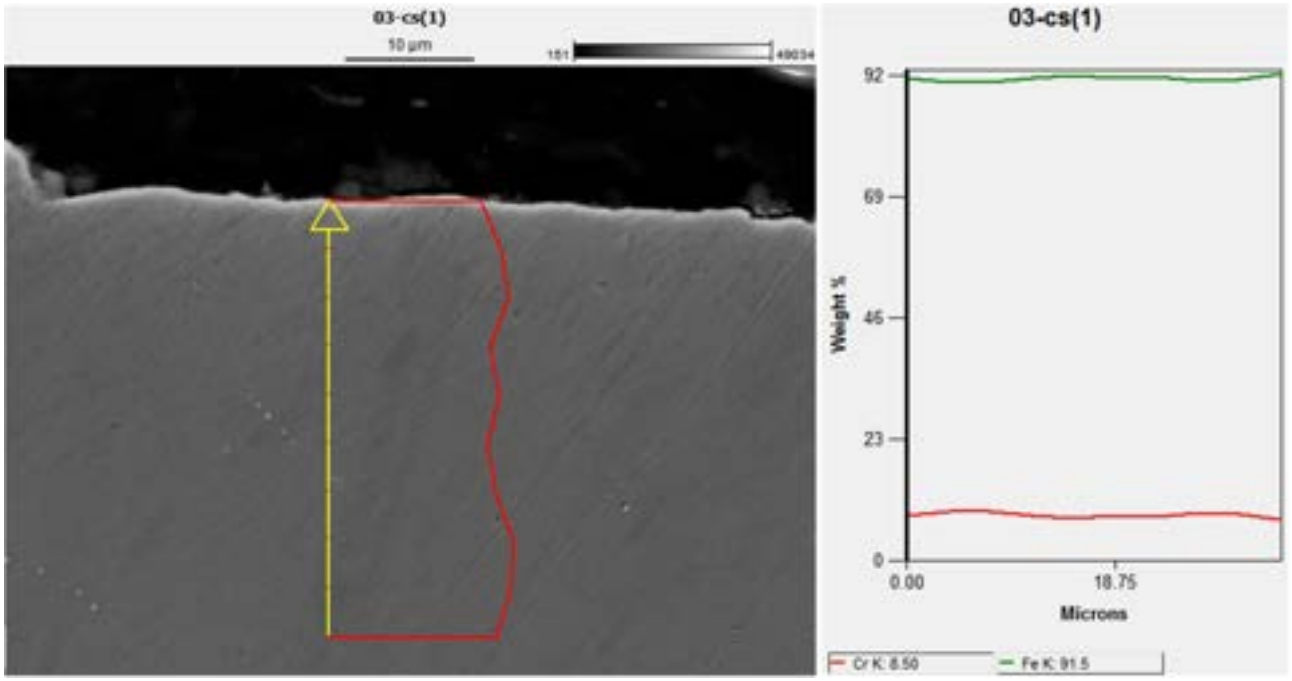

Figure 39: left: SEM image and Cr concentration profile (EDS) of specimen n°3 cross section; right: Cr (red) and Fe (green) concentration profiles along the specimen section.

Figure 40 shows on the left a SEM representative image of specimen n° 4 section, with the red Chromium concentration profile overlapped, as determined by the EDS analysis; on the right side is instead reported a graph showing the profiles of both Chromium and Iron elements. The graph meaning and details are the same already described for Figure 37. No internal morphological damage is evident; the concentration profiles are rather flat, with perhaps a minimal Cr concentration decrease in the first microns below the surface; small fluctuations are anyway due to the uncertainty in the EDS analysis result.

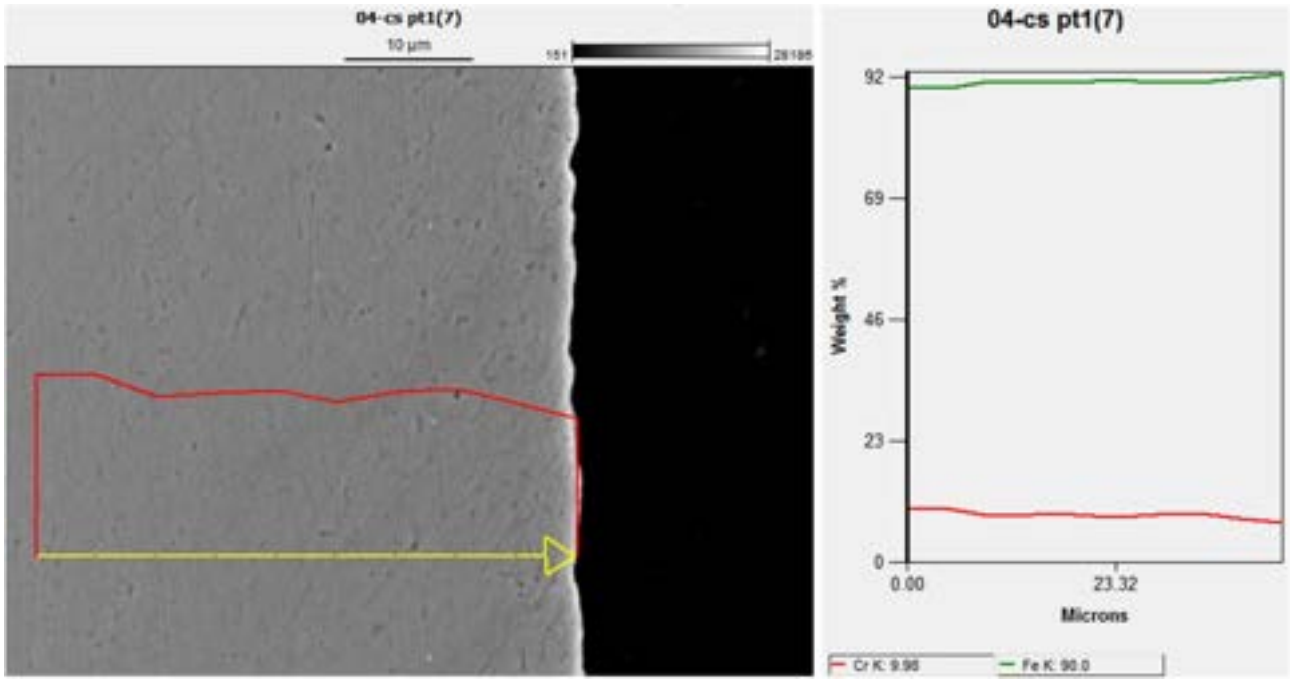

Figure 40: left: SEM image and Cr concentration profile (EDS) of specimen n°4 cross section; right: Cr (red) and Fe (green) concentration profiles along the specimen section.

Finally, Figure 41 shows on the left a SEM representative image of specimen n° 5 section, with the red Chromium concentration profile overlapped, as determined by the EDS analysis; on the right side is instead reported a graph showing the profiles of both Chromium and Iron elements. The graph meaning and details are the same already described for Figure 37. No internal morphological damage is evident; the concentration profiles are rather flat, with small fluctuations due to the uncertainty in the EDS analysis result.

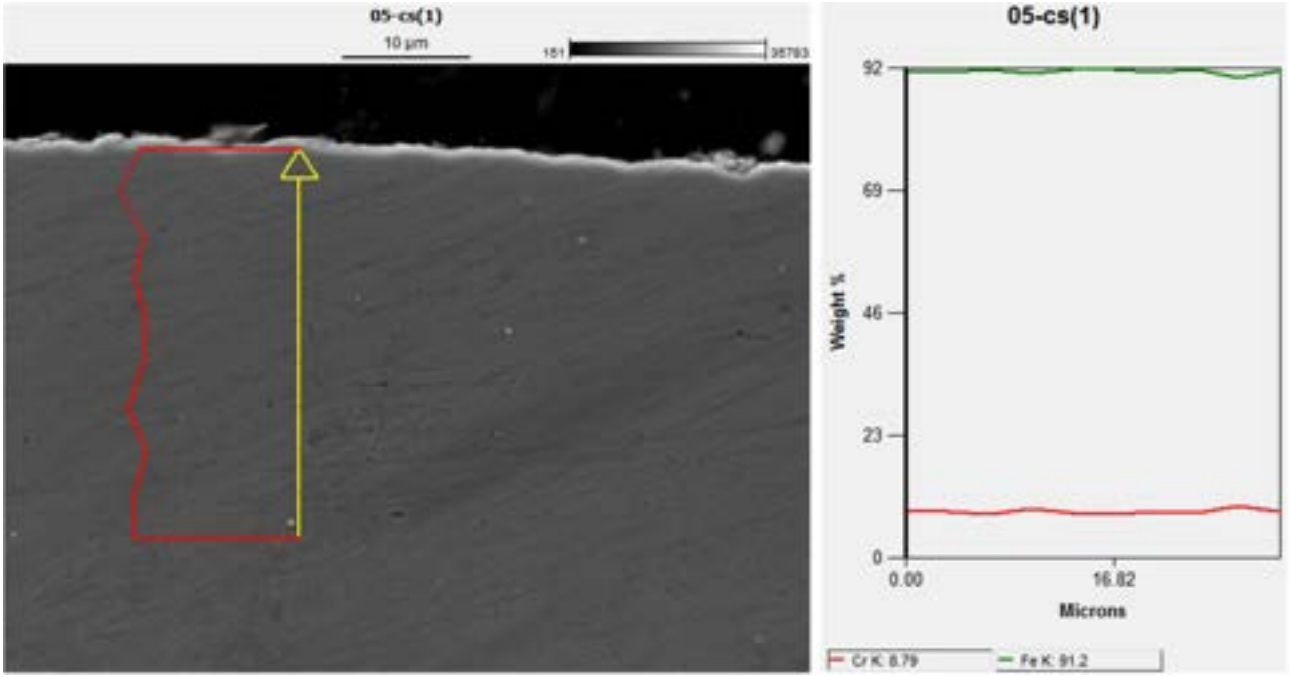

Figure 41: left: SEM image and Cr concentration profile (EDS) of specimen n°5 cross section; right: Cr (red) and Fe (green) concentration profiles along the specimen section.

Now, let's consider the F82H specimens, starting with the one not submitted to the erosion-corrosion action by the flowing liquid Lithium (fresh specimens, no 31).

Figure 42 shows on the left a SEM representative image of specimen n° 31 section, with the red Chromium concentration profile overlapped, as determined by the EDS analysis; on the right side is instead reported a graph showing the profiles of both Chromium and Iron elements. The graph meaning and details are the same already described for Figure 37.

From the observation of the Figure, it is possible to note that the internal specimen structure is in good condition, with only some sign due to the cut and preparation of the sample, but no erosion-corrosion damage: this is of course what expected, since specimen n° 31 is an unexposed specimen. The concentration profiles indicate a substantial constancy of values, with minimal fluctuations due to the uncertainty in the EDS analysis result.

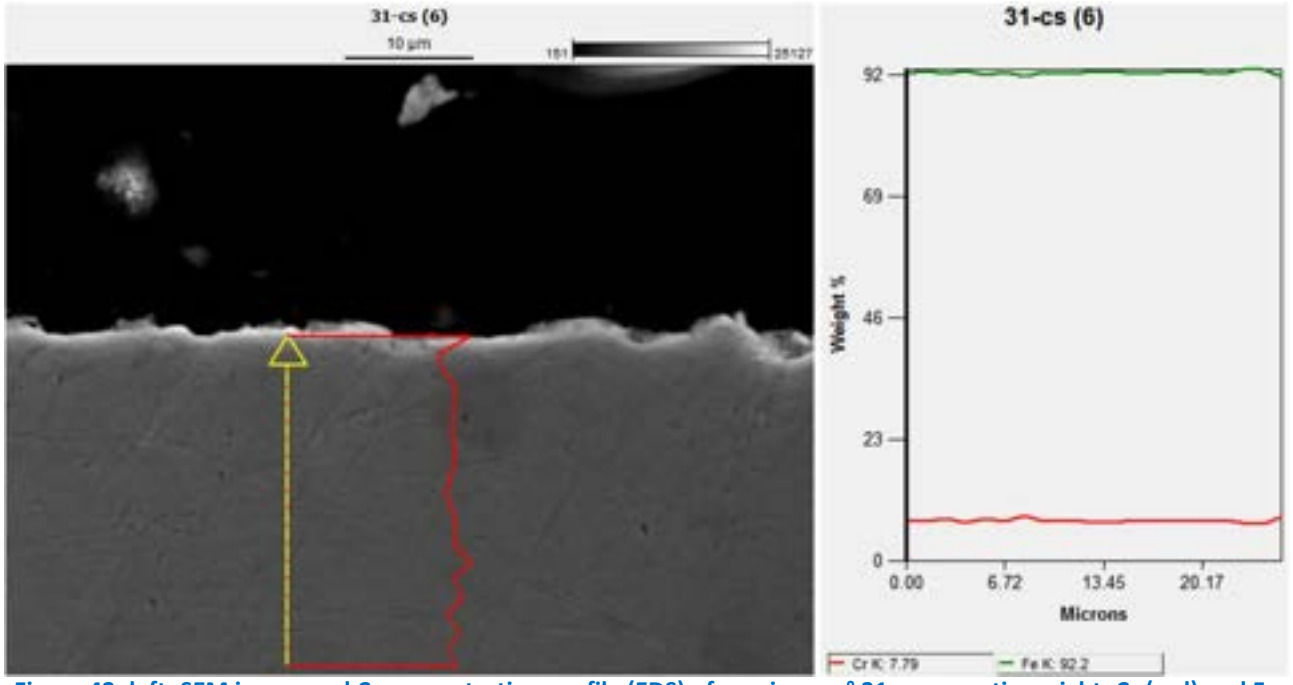

Figure 42: left: SEM image and Cr concentration profile (EDS) of specimen n° 31 cross section; right: Cr (red) and Fe (green) concentration profiles along the specimen section.

Figure 43 shows on the left a SEM representative image of specimen n° 23 section, with the red Chromium concentration profile overlapped, as determined by the EDS analysis; on the right side is instead reported a graph showing the profiles of both Chromium and Iron elements. The graph meaning and details are the same already described for Figure 37. No internal morphological damage is evident; the concentration profiles are rather flat, with small oscillations due to the uncertainty in the EDS analysis result.

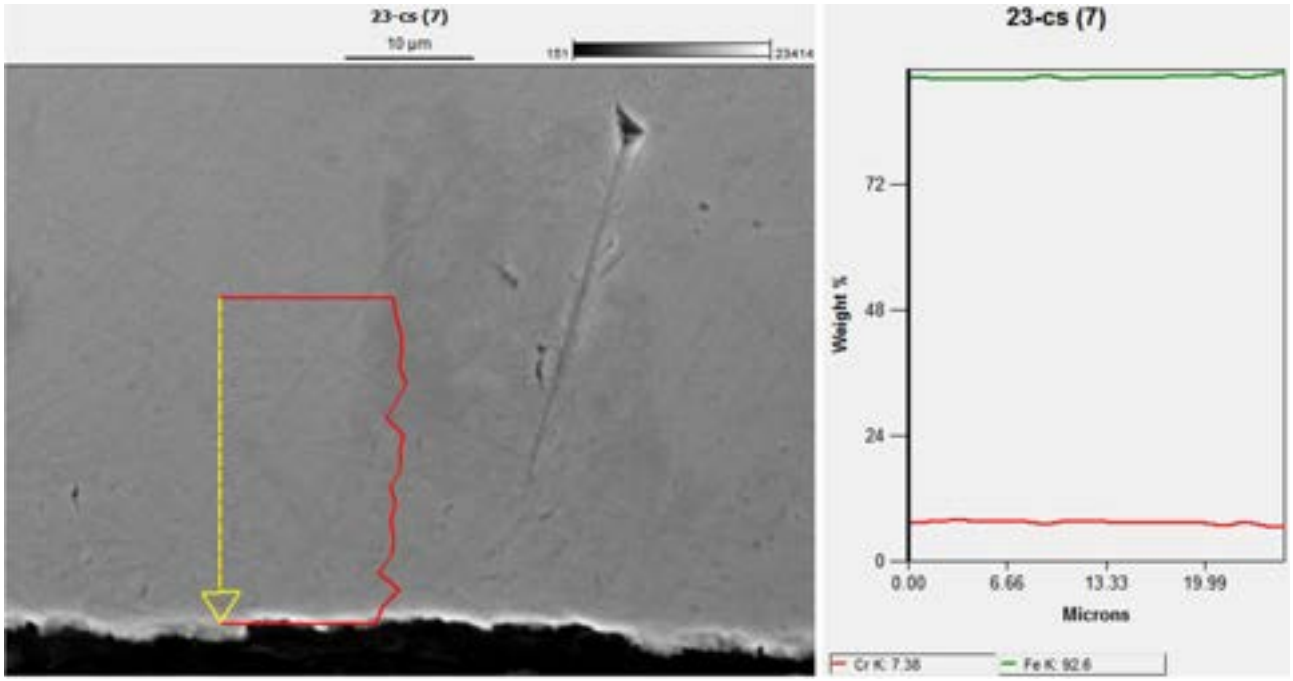

Figure 43: left: SEM image and Cr concentration profile (EDS) of specimen n° 23 cross section; right: Cr (red) and Fe (green) concentration profiles along the specimen section.

Figure 44 shows on the left a SEM representative image of specimen n° 24 section, with the red Chromium concentration profile overlapped, as determined by the EDS analysis; on the right side is instead reported a graph showing the profiles of both Chromium and Iron elements. The graph meaning and details are the same already described for Figure 37. No internal morphological damage is evident; the concentration profiles are rather flat, with only a small positive peak in Cr concentration at about half path, due to the uncertainty in the EDS analysis result or to a local concentration which is higher by chance. A corresponding peak is visible also in the Fe profile, this time negative, since the sum of the two concentration values is fixed to be always 100%. In any case, no real increasing/decreasing trend appears moving along the direction of the yellow arrow.

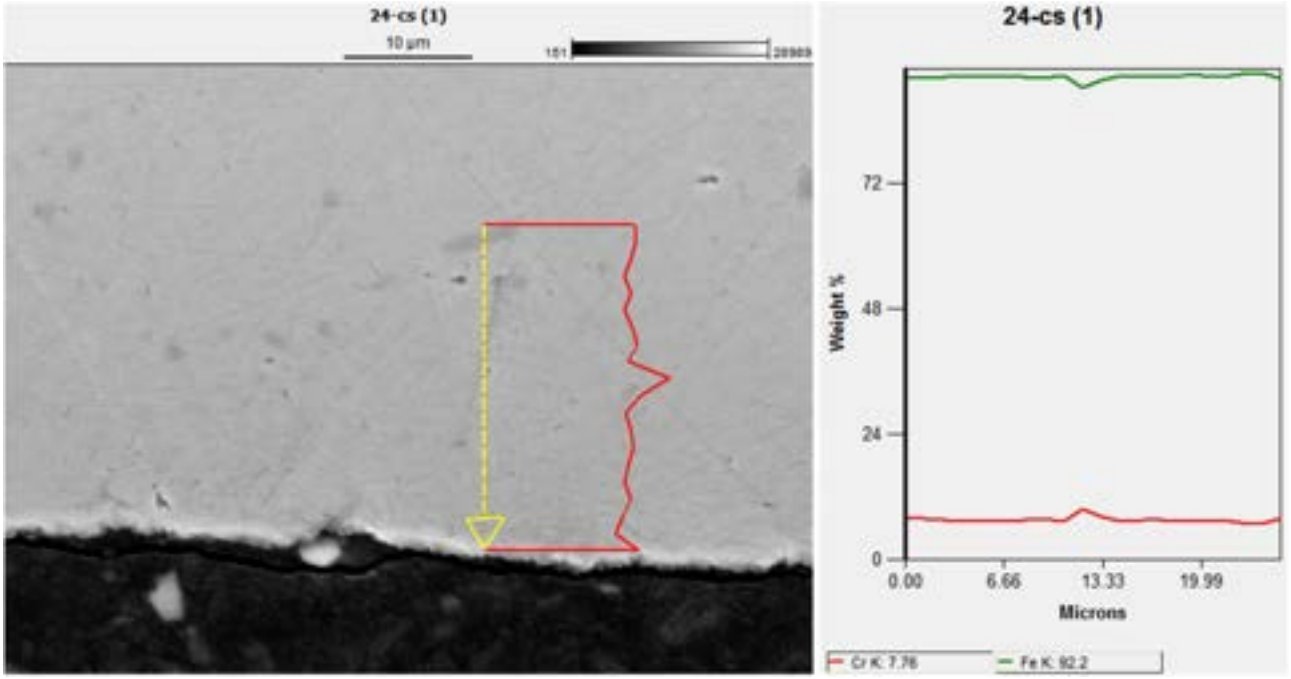

Figure 44: left: SEM image and Cr concentration profile (EDS) of specimen n° 24 cross section; right: Cr (red) and Fe (green) concentration profiles along the specimen section.

Figure 45 shows on the left a SEM representative image of specimen n° 25 section, with the red Chromium concentration profile overlapped, as determined by the EDS analysis; on the right side is instead reported a graph showing the profiles of both Chromium and Iron elements. The graph meaning and details are the same already described for Figure 37. No internal morphological damage is evident; the concentration profiles are rather flat, with minimal oscillations due to the uncertainty in the EDS analysis result.

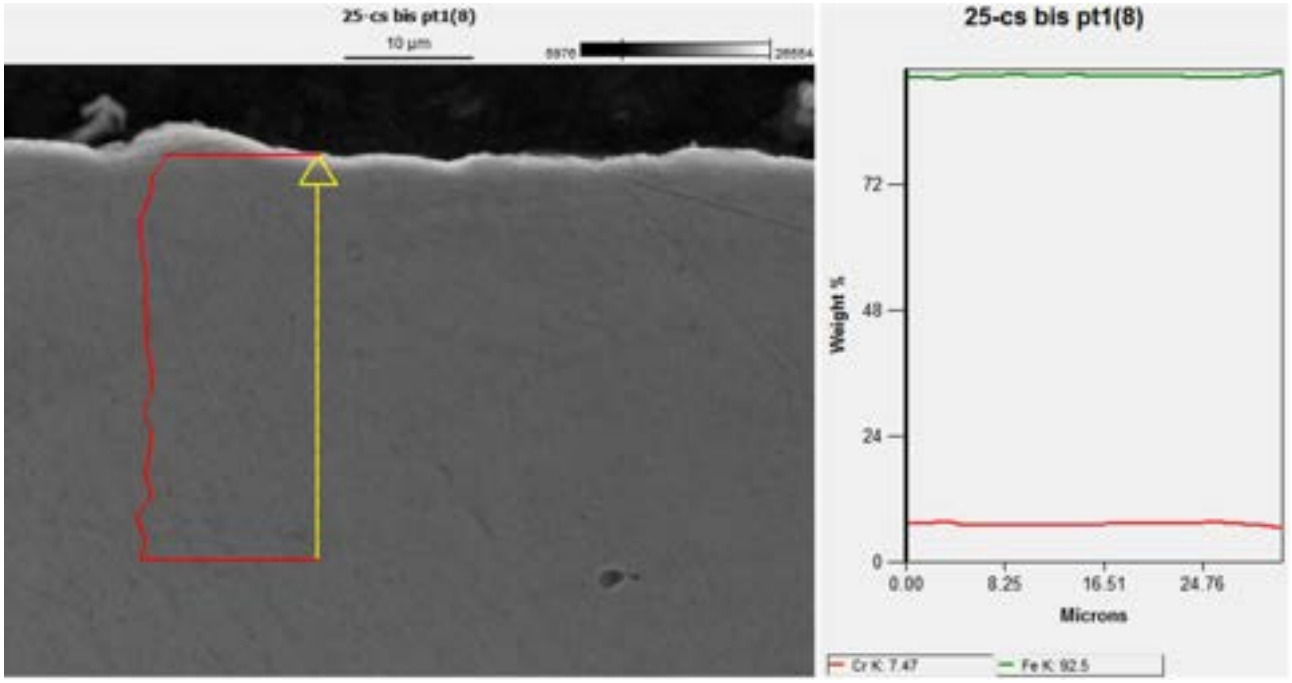

Figure 45: left: SEM image and Cr concentration profile (EDS) of specimen n° 25 cross section; right: Cr (red) and Fe (green) concentration profiles along the specimen section.

Finally, Figure 46 shows on the left a SEM representative image of specimen n° 26 section, with the red Chromium concentration profile overlapped, as determined by the EDS analysis; on the right side is instead reported a graph showing the profiles of both Chromium and Iron elements. The graph meaning and details are the same already described for Figure 37. Apart from the signs produced during the cut and the preparation of the sample, no internal morphological damage is evident; the concentration profiles are rather flat, with small oscillations due to the uncertainty in the EDS analysis result.

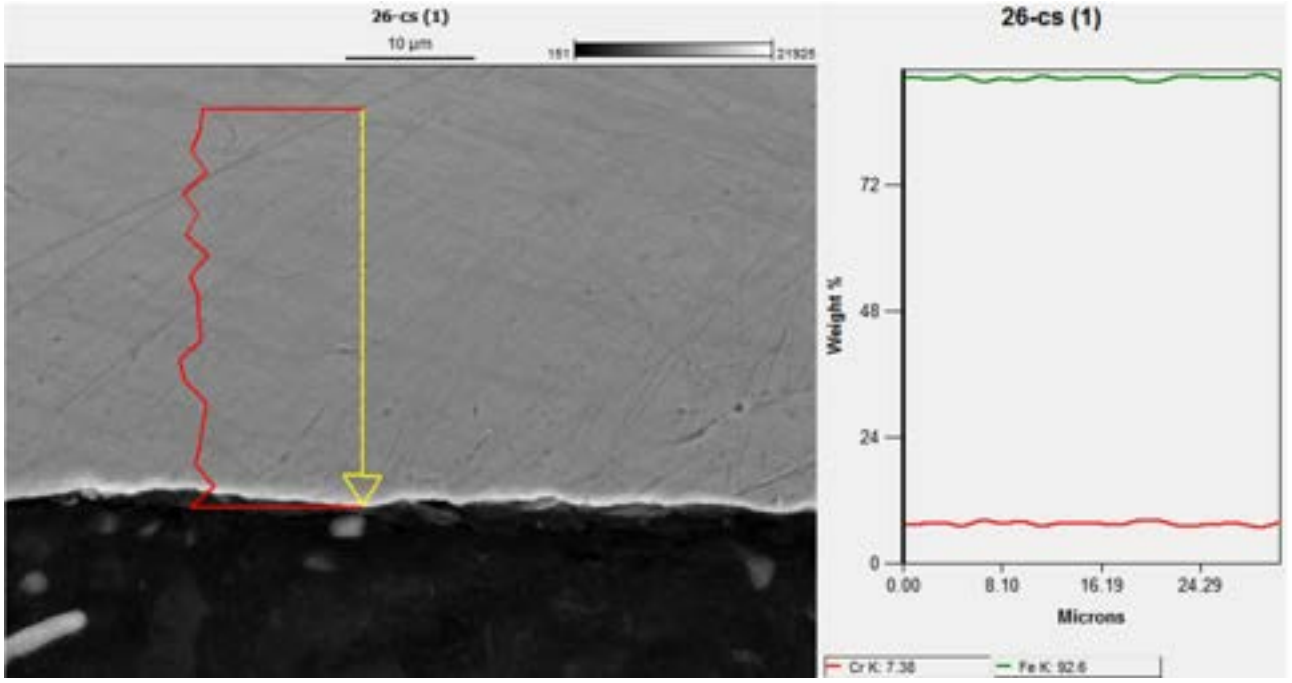

Figure 46: left: SEM image and Cr concentration profile (EDS) of specimen n° 26 cross section; right: Cr (red) and Fe (green) concentration profiles along the specimen section.

From the ensemble of figures reported in this section (37-45), it can be concluded that no structural/morphological damage was produced on the investigated specimen by the action of flowing liquid Lithium.

The composition versus depth (distance from the surface) profiles do not indicate a significant trend in concentration values. The only difference between the fresh and the exposed specimen might be, in some cases, a smaller average value of Cr concentration in the exposed ones, in accordance with Table 16 results . In any case, the uncertainty in the EDS analysis result is to high respect to the Cr concentration variations to permit an accurate description of the profile and to calculate the thickness of a possible Cr depleted layer in the neighbourhood of the surface.

2.4.7 Optical microscope inspection of the specimens section after the chemical etching

In order to enhance the inner intergranular structure of the specimens and the possible damages produced by the erosion-corrosion short term test (like for instance grain detachment, anomalies at the grain boundaries,…), after the SEM-EDS analysis the specimens cross sections have been submitted to a chemical etching treatment, employing Nital at room temperature for 90 seconds. The so obtained samples have been observed with Nikon Eclipse optical microscope (polarized light) at 500 enlargements. Below are reported all the images this way obtained.

First of all, let's consider the Eurofer 97 specimens, starting with the one not submitted to the erosion-corrosion action by the flowing liquid Lithium (fresh specimens, n° 10). Figure 47 is an optical microscope images of the section, obtained in a region close to the exposed surface.

The material present a fine, equigranular structure, with grains having dimensions on the order of 10 µm. This value agrees with the expected (commonly reported in literature) one. No meaningful differences appear between the inner region and the region close to the surface.

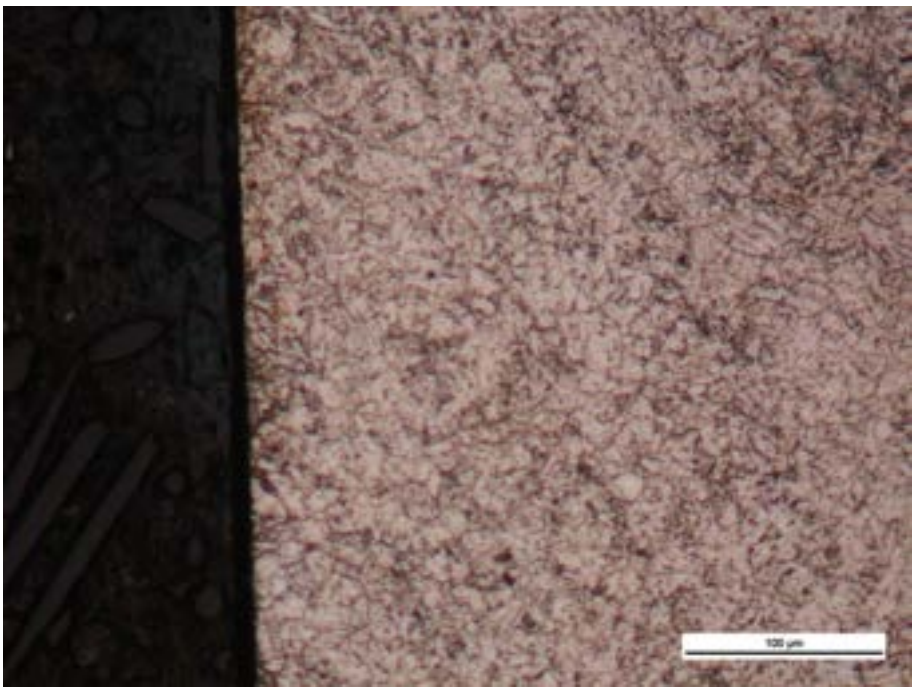

Figure 47: optical microscope image of the specimen n°10 cross section, after the chemical etching: detail of a region close to the exposed surface (black area on the left is the supporting resin).

Next Figures 48 to 51 report instead the optical microscope images of the tested Eurofer 97 specimens (n° 2, n° 3, n° 4, n° 5). By comparing these images with the ones of the unexposed specimen, it can be stated that the grain structure of the tested specimen was not significantly affected by the 1222 hours of exposure to flowing Lithium. Particularly, the grains at the surfaces were not removed or evidently modified.

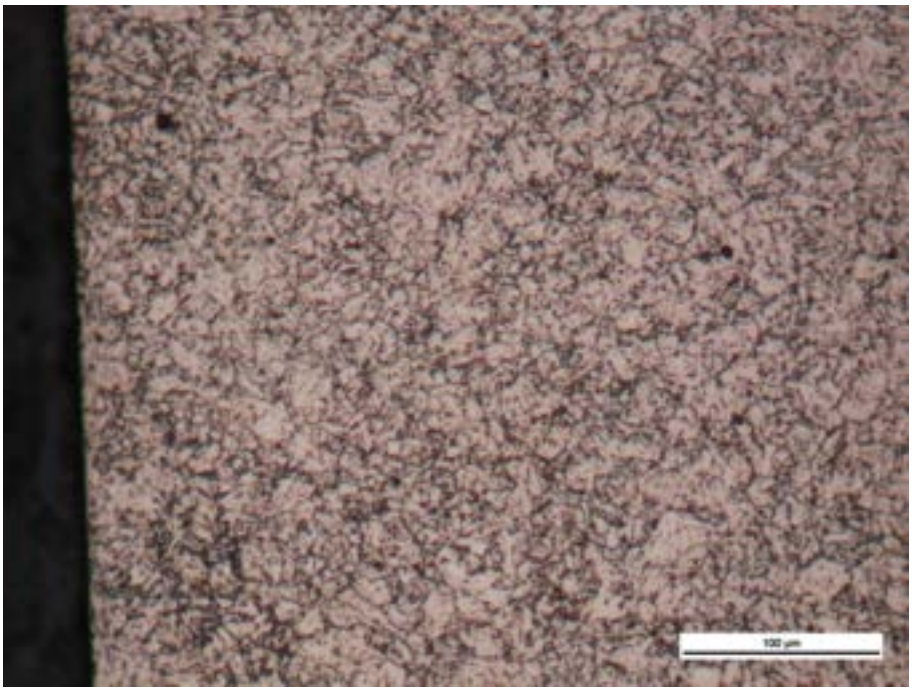

Figure 48: optical microscope image of the specimen n° 2 cross section, after the chemical etching: detail of a region close to the exposed surface (black area on the left is the supporting resin).

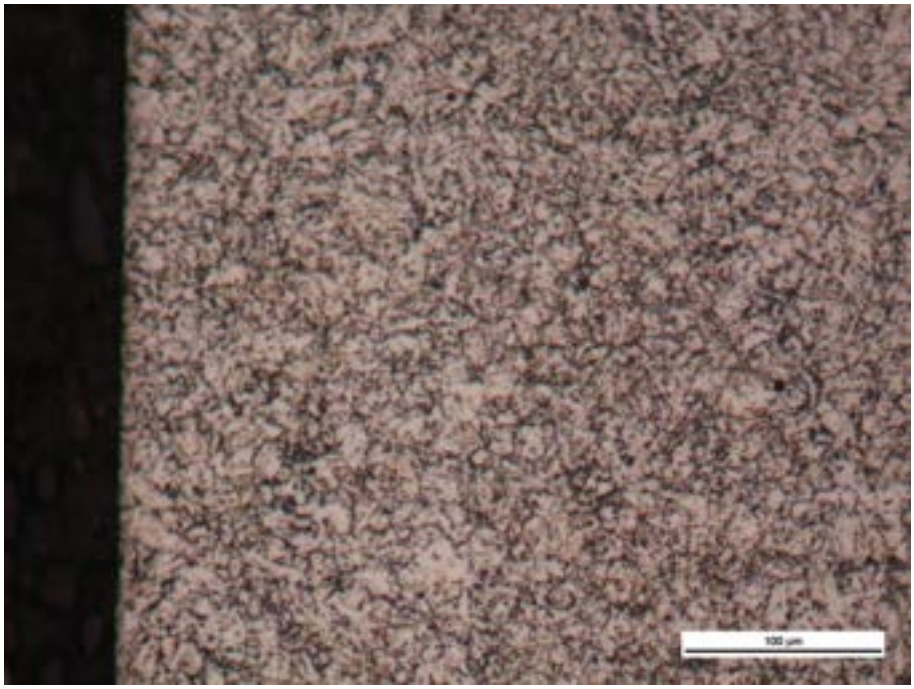

Figure 49: optical microscope image of the specimen n° 3 cross section, after the chemical etching: detail of a region close to the exposed surface (black area on the left is the supporting resin).

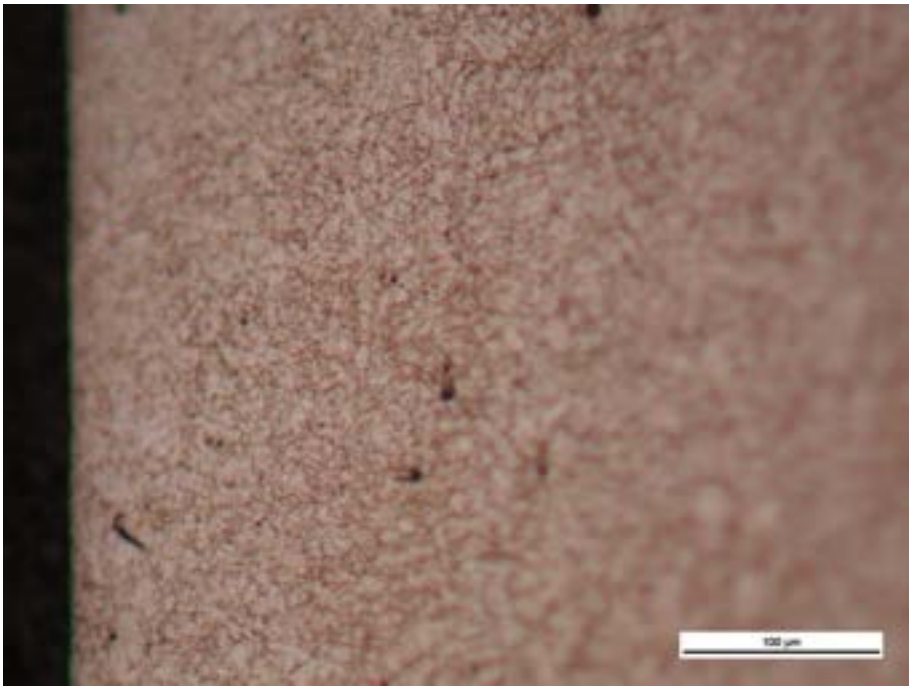

Figure 50: optical microscope image of the specimen n° 4 cross section, after the chemical etching: detail of a region close to the exposed surface (black area on the left is the supporting resin).

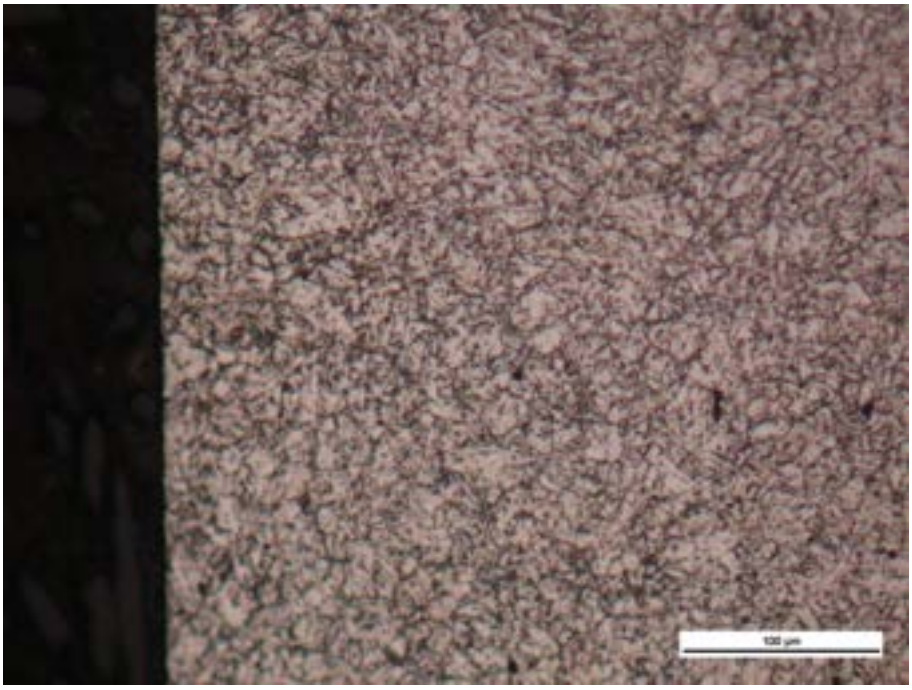

Figure 51: optical microscope image of the specimen n° 5 cross section, after the chemical etching: detail of a region close to the exposed surface (black area on the left is the supporting resin).

Let's consider now the F82H specimens, starting with the one not submitted to the erosion-corrosion action by the flowing liquid Lithium (fresh specimens, n° 31). Figure 52 is the optical microscope image of the section, obtained in a region close to the exposed surface of the sample.

The material present a granular structure different from Eurofer 97 one, being characterized on average by much larger grains (about 50-100 µm), which result, therefore, more clearly visible. Such a grain structure agrees with what expected for the F82H material. No meaningful differences appear between the inner region and the region close to the surface.

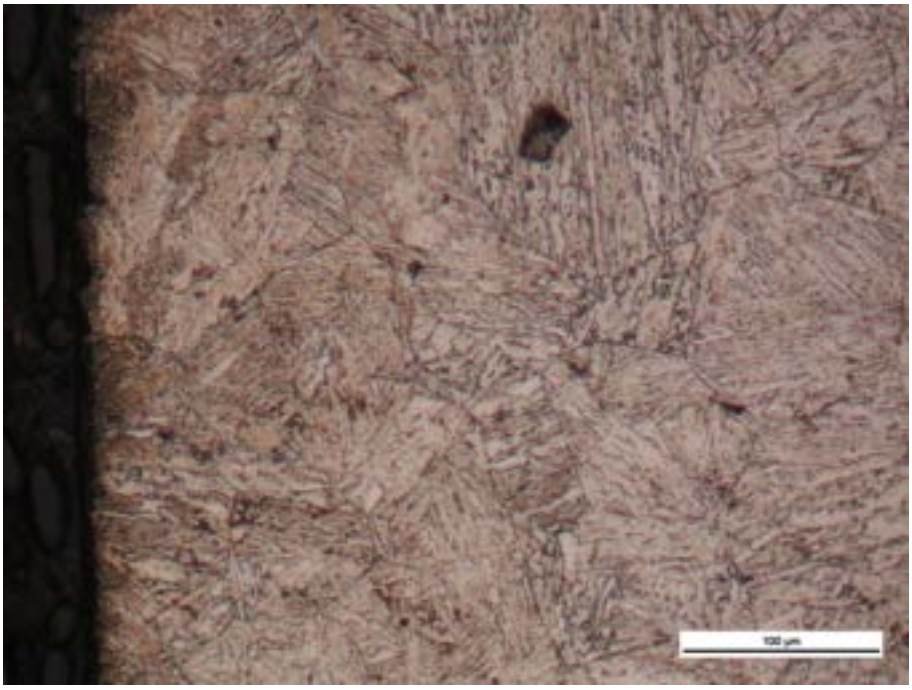

Figure 52: optical microscope image of the specimen n° 31 cross section, after the chemical etching: detail of a region close to the exposed surface (black area on the left is the supporting resin).

Next Figures 53 to 56 report instead the optical microscope images of the tested F82H specimens (n° 23, n° 24, n° 25, n° 26). By comparing these images with the ones of the unexposed specimen, it can be stated that the grain structure of the tested specimen was not significantly affected by the 1222 hours of exposure to flowing Lithium. Particularly, the grains at the surfaces were not removed or evidently modified.

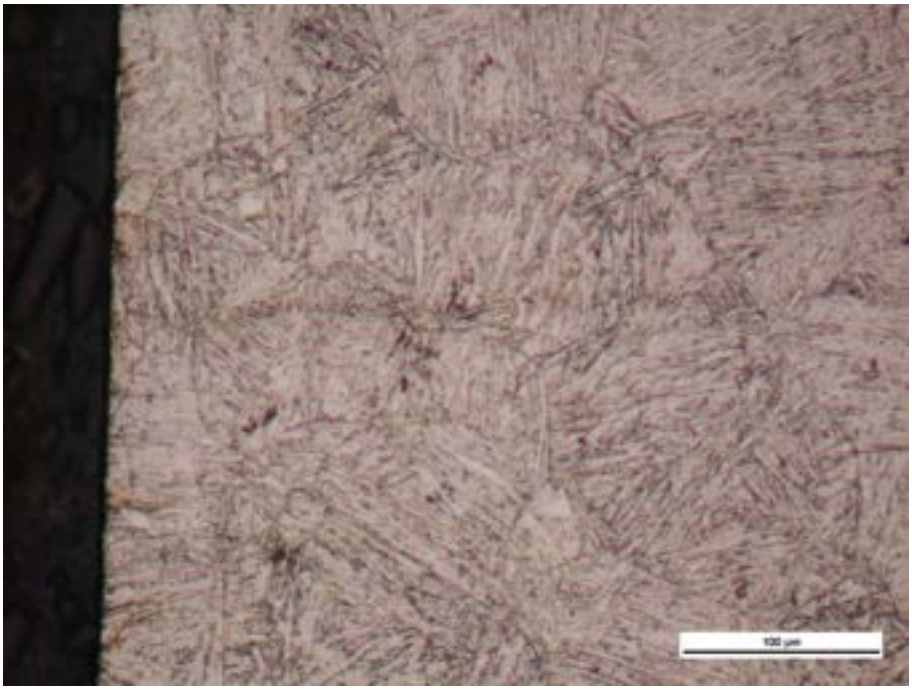

Figure 53: optical microscope image of the specimen n° 23 cross section, after the chemical etching: detail of a region close to the exposed surface (black area on the left is the supporting resin).

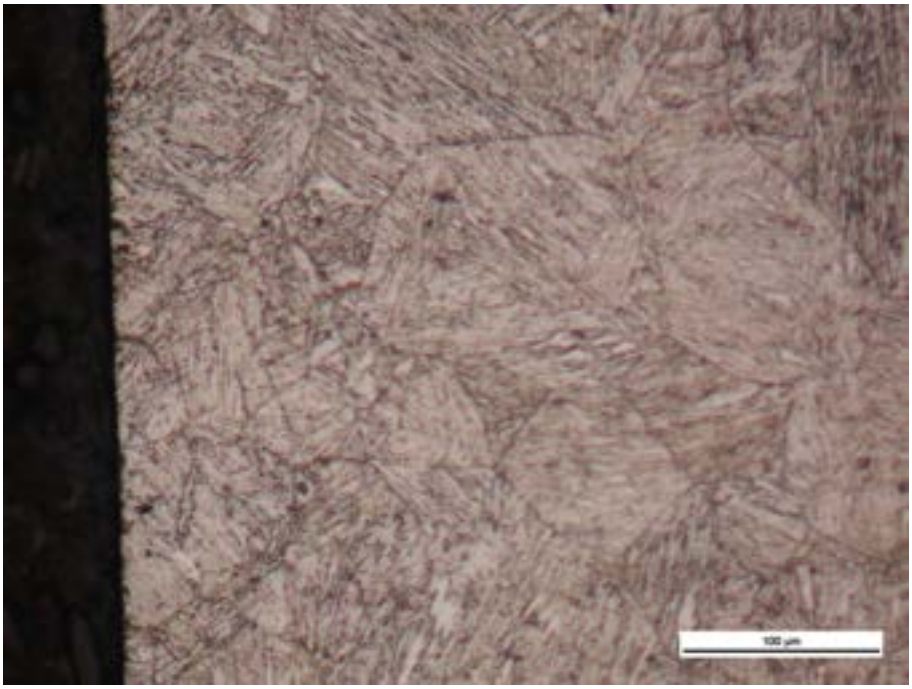

Figure 54: optical microscope image of the specimen n° 24 cross section, after the chemical etching: detail of a region close to the exposed surface (black area on the left is the supporting resin).

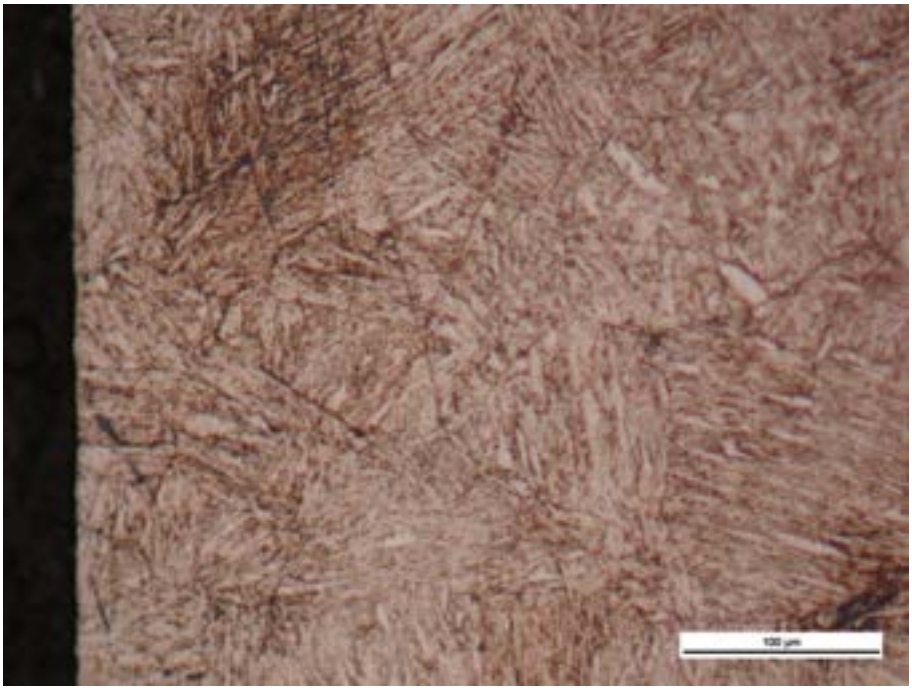

Figure 55: optical microscope image of the specimen n° 25 cross section, after the chemical etching: detail of a region close to the exposed surface (black area on the left is the supporting resin).

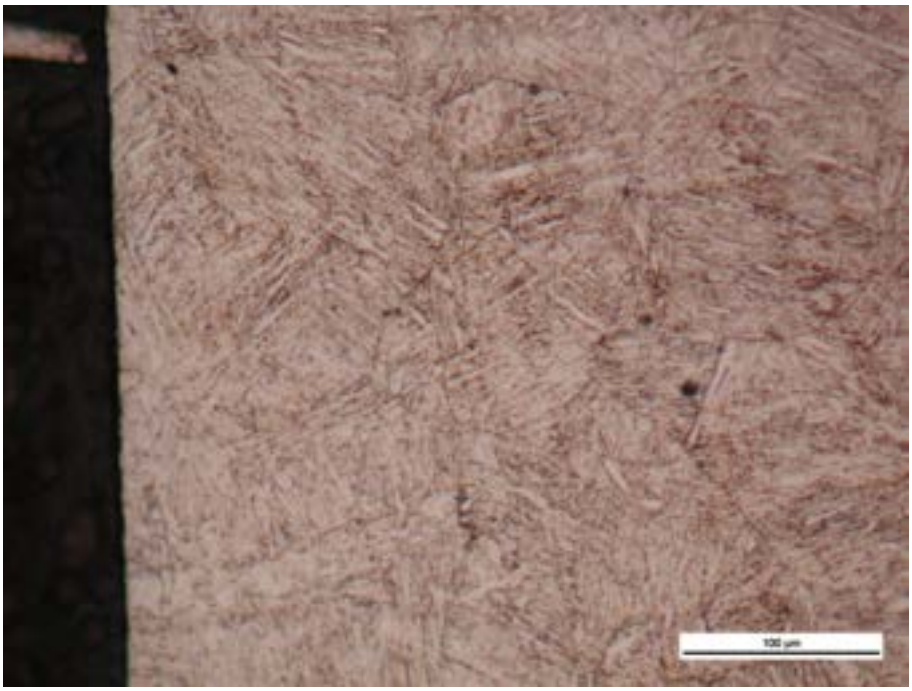

Figure 56: optical microscope image of the specimen n° 26 cross section, after the chemical etching: detail of a region close to the exposed surface (black area on the left is the supporting resin).

2.5 *Analysis of the specimens after the mid term test: generalized corrosion rates*

As anticipated in section 1, only a partial evaluation of the specimens behaviour during the mid term test (2000 hours exposure) is possible at the moment, being the chemical and metallographic analyses still ongoing. This partial assessment is based on the specimens registered mass variations. They are reported in Table 17, together with the corresponding calculated generalized corrosion rate.

Table 17: mass variation and generalized corrosion rate for the mid term specimens

Material	Specimen identification	Mass variation [mg]	Corrosion rate [µm/y]
Eurofer 97	6	- 0.08 ± 0.03*	0.09 ± 0.03
Eurofer 97	7	- 0.01 ± 0.03	0.01 ± 0.03
Eurofer 97	8	+ 0.01 ± 0.03	< 0.03
Eurofer 97	9	- 0.06 ± 0.03	0.07 ± 0.03
F82H	27	- 0.12 ± 0.03	0.13 ± 0.03
F82H	28	+ 0.04 ± 0.03	< 0.03
F82H	29	- 0.02 ± 0.03	0.02 ± 0.03
F82H	30	- 0.69 ± 0.03	0.76 ± 0.03

* ± 0.03 mg is the Standard Deviation of the weighing process

All the specimens, except one, are characterized by a very small weight loss, aligned to the ones calculated for the Short Term Test (Table 5); considering that in this second test the exposure time is larger (2000 hours instead of 1222), the maximum corrosion rate results even smaller.

Specimen #30 suffers instead a large weight loss, which translates into a rather high rate (0.76 µm/y). It must be said that this specimen had been positioned at the entering of the Test Section (top of the column; see Figure 57 for specimens disposal), where the sudden narrowing of the Lithium path could have generated a swirling flow and turbulences, producing therefore a remarkable increase of the erosive action of the liquid compared to the rest of the Test Section. It is also true, however, that during the Short Term Test a similar difference had not been observed and all the 8 specimens had been characterized by a similar (and good) experimental answer. Specimen #30 anomaly could be better understood once all the chemical and metallographic analyses will be completed.

Figure 57: scheme of specimens disposal inside the Test Section for the mid term test.

3 Conclusioni

Eight specimens have been submitted to the erosion-corrosion short term test (1222 hours of exposure to flowing liquid Lithium) employing Lifus 6 plant, half made of Eurofer 97, half made of F82H. The many analysis performed on the specimens, also based on the comparison between the fresh and the tested ones, all indicate that no significant damage was produced on them by the exposure to Lithium: all the specimens present, after the test, a smooth and regular surface, not different from that at the beginning; the roughness parameters (Ra, Rz) were essentially not changed by the test; the physical dimensions (height and diameter) were left identical; the morphological (SEM) inspection of both the exposed surface and the cross section of the specimens shows no sign of alteration provoked by erosion-corrosion mechanism; the optical microscope inspection of the cross section after a chemical etching treatment, again indicates no grain detachment or modification to the intergranular structure of the specimens, both close to the surface and in the bulk.

The EDS analysis permitted to evaluate the chemical composition of the alloys at the surface (average of a large surface area) and in discrete equidistant points below the surface (few microns one from the other), constructing composition vs depth profiles. Even if an uncertainty of ± ~ 0.5 wt % in the concentration results cannot be avoided with the EDS analysis, it seems that maybe some Tungsten (W) diminution occurred at the surface as consequence of the test, while almost surely this occurred to Chromium (Cr): this element decreased in all the exposed specimens, with a minimum diminution of 0.6 wt % and an average one (considering all the specimens) of ~ 1 wt %. The composition versus depth profiles has not show instead a significant trend in concentration values: a small inhomogeneity could be actually present in a submicron (or very few microns) layer below the exposed surface, but to characterize this very thin specimen thickness some additional and more specific technique would be necessary.

Elements different from the ones in the starting alloy composition (like C, O, N, other metals…) have been not found, a part from very few cases in restricted positions, which have been anyway ascribed to the sample contamination during its handling, preparation or post test-treatment, but no the test itself. This evidence has permitted to give consistency to the calculated mass variations of the specimens, in that these values result only from the real amounts of dissolved alloys, being not compensated by a possible adsorption or insertion of extern material.

The maximum registered mass diminution was ~ 0.13 mg (for both the steels), which corresponds, taken into account the geometry of the specimens and the density of the materials, to a maximum generalized corrosion rate of ~ 0.23 µm/y. No meaningful difference has been noted between Eurofer 97 and F82H corrosion rates.

For what concerns the mid term test (2000 hours of exposure), eight new fresh specimens have been investigated, four for each of the two materials. Only their mass variations have been registered at the moment, being still ongoing their deep chemical and metallographic investigations. The mass diminutions have been again very small, aligned to the short term test and translating into an even smaller maximum corrosion rate (~ 0.13 µm/y), in view of the longer exposure time. Just one specimen anyway, the one located in the top position, at the entering of the Test Section, exhibited remarkably higher mass diminution and corresponding corrosion rate (~ 0.76 µm/y): maybe this fact could be ascribed to the particular flow condition in the specific location of that specimen, where flow turbulences might be significant.

On the whole, it can be concluded that the tests results are quite comforting, since the measured corrosion rates are significantly smaller than the corrosion rate limit set for IFMIF (1 µm/y).

4 Riferimenti bibliografici

1. A. Tincani, A. Aiello, S. Mannori, C. Lenzi, G. Fasano, M. Muzzarelli “Realizzazione e qualifica dell’impianto sperimentale per prove di corrosione/erosione in litio (LIFUS6)”, Report Rds/PAR2013/, Settembre 2013
2. P. Favuzza, G. Fasano, S. Mannori, M. Tarantino, A. Tincani “Rapporto finale sulla realizzazione e commissioning dell’impianto Lifus 6 per lo studio dei fenomeni di erosione/corrosione”, Report RdS/PAR2013/208, Settembre 2014
3. IFMIF International Team “IFMIF Comprehensive Design Report”, 2004
4. P.Agostini “Corrosion/erosion of steels in Lithium: LIFUS3 tests”, Enea Report IM-A-R-004, 25/2/2008
5. P.Favuzza, A.Aiello, A. Tincani, M.Muzzarelli, “Engineering Design Report of Lifus 6 Purification System”, IFMIF/EVEDA Deliverable LF 4.4.1, January 2014
6. P.Favuzza, S.Mannori “Acceptance Test Report of the Lifus 6 Purification System”, IFMIF/EVEDA Deliverable LF 4.4.3, May 2015
7. P.Favuzza, “Rapporto sulla validazione del sistema di purificazione del litio all’interno di Lifus 6 e del sistema di monitoring online di tali impurezze”, Report Rds/2013/126, settembre 2013
8. P.Favuzza, A.Antonelli, M.Cuzzani, G.Fasano, S.Mannori, “Risultati relativi alla prima fase di purificazione del Litio circolante all'interno dell'impianto Lifus 6 e verifica ed ottimizzazione contestuale del suo funzionamento”, Report Rds/2014/055, settembre 2015
9. P.Favuzza, “Delivery of F82H and Eurofer Steel for Test of Specimens”, IFMIF/EVEDATechnical Note LF3 NP-1, March 2013
10. P.Favuzza, “Phase I Validation Report of the Lifus 6 Purification System”, IFMIF/EVEDA Deliverable LF 4.5.1, December 2015
11. P.Favuzza, “Final Validation Report of the Lifus 6 Purification System”, IFMIF/EVEDA Deliverable LF 4.5.2, April 2016

5 Abbreviazioni ed acronimi

d_e	External diameter
EDS	Energy Dispersive X-ray Spectrometry
h	height
IFMIF	International Fusion Materials Irradiation Facility
Ra, Rz	Rugosity Parameters
RAFM	Reduced Activation Ferritic Martensitic
SEM	Scannin Electron Microscopy
Std dev	Standard Deviation
wppm	Weight Parts per Million